

Additional Methods for Tailless Aircraft Conceptual Design

Gregory W. Page¹

Naval Air Warfare Center, Aircraft Division, Patuxent River, MD, 20650

The complexity of the conceptual design of tailless aircraft can appear daunting to many. The multiple design aspects that are able to be broken out into individual problems on conventional designs, are all interrelated on the tailless aircraft configuration. This paper documents additional methods for tailless aircraft design for aspect ratios ≤ 10 , and sweep angles $\leq 45^\circ$. These methods are based upon well known references that should be readily available to any designer during the conceptual design phase. Since better tools exist in the major design houses, it's assumed that a majority of conceptual designers using these methods would be homebuilt aircraft enthusiasts or modellers.

Nomenclature

A	=	wing aspect ratio
c'	=	wing mean aerodynamic chord
C_{DL}	=	wing drag coefficient due to lift
C_L	=	wing lift coefficient
c_{ℓ_α}	=	airfoil section lift curve slope
C_m	=	wing pitching moment coefficient
C_{m_0}	=	wing zero-lift pitching moment coefficient
$(C_{m_0})_{\theta=0}$	=	wing zero-lift pitching moment coefficient with zero twist
$\frac{\Delta C_{m_0}}{\theta}$	=	change in wing zero-lift pitching-moment coefficient due to a unit change in linear wing twist
c_{m_0}	=	airfoil zero-lift pitching moment coefficient
$\frac{dC_m}{dC_L}$	=	static margin ($-x/c'$)
e	=	Oswald span efficiency
M	=	Mach number
v	=	induced-drag factor due to linear twist
w	=	zero-lift drag factor due to linear twist
x	=	distance from the center of gravity to the aerodynamic center
β	=	compressibility factor ($\sqrt{1-M^2}$ for subsonic)
θ	=	wing twist (positive for washin, negative for washout)
$\Lambda_{c/4}$	=	wing sweep measured at the $1/4$ chord point
λ	=	wing taper ratio
γ	=	compressibility correction factor to the wing zero-lift pitching moment coefficient $((C_{m_0})_M / (C_{m_0})_{M=0})$

¹ Aerospace Engineer, Systems Engineering Dept., 48110 Shaw Rd., Patuxent River MD, 20670. gregory.page@navy.mil

I. Introduction

WHILE the practicality and overall efficiency of the tailless aircraft configuration has been an ongoing debate, the perceived simplicity and beauty of these aircraft has captured the imagination of many aviation enthusiasts. The design of the tailless aircraft has proved to be a fascination of the aviation community since before WWII, and the work of the Horten brothers, Alexander Lippisch, Jack Northrop and a myriad of other designers have been the subject of numerous books and papers. However, most of these focus on the aircraft themselves, and not on how the design was achieved. The number of references appropriate for conceptual and detailed design of tailless aircraft is fairly limited. This paper is intended to provide additional methods for tailless aircraft conceptual design and assist in filling a portion of that gap.

II. The Problem of Tailless Aircraft Conceptual Design

While a Senior at North Carolina State University in 1989, the author's design team was presented a requirement for an Unmanned Aerial Vehicle (UAV) that was required to be a tailless aircraft configuration. At the time, NC State required it's Aerospace Engineering students to design their configuration during the Fall Semester, and build and fly a radio-controlled subscale version in the Spring Semester. The design problem within a single semester appeared almost insurmountable. This was largely caused by the limited availability of design documentation in the pre-internet age, combined with complexity of trying to balance wing sweep, twist, taper ratio, airfoil pitching moment, and the configuration center-of-gravity to achieve minimum induced drag, trim, and acceptable levels of stability.

Without a suitable solution linking airfoil pitching moment requirements to minimum induced drag and trim, the University's Aerospace Lab Coordinator designed a set of low pitching moment root and tip airfoils for the three design teams using the EPPLER code. These were then used in the team's VSAERO models to achieve trim without regard to the minimum induced drag of the configuration. The author encountered this problem again when working with a colleague on the XUV configuration in the 1994 timeframe with much the same results.



Figure 1. Author's Senior design project; Crossbow.

Since that time, the author continued to search tailless aircraft design references for a simple method relating wing twist, sweep, aspect ratio, taper ratio, airfoil pitching moment, and minimum induced drag. While a number of methods were encountered, they either utilized a bell shaped approach to the lift distribution, or the derivation (and hence accuracy) of the methods were unknown. As the years passed, the author continued to return to the problem of tailless aircraft design to determine if any new references had become available to answer this question. As is often the case, we sometimes find the answer to a problem when we aren't looking for it. While the author was assisting a friend with a conceptual design effort on a conventional configuration, he realized that the answer to one of his major questions had been sitting on his book shelf for over a decade.

III. Minimum Taper Ratio

The determination of the basic planform of the tailless aircraft conceptual design has many considerations that are beyond the scope of this paper. The selection of the wing span and area are largely design and mission specific, and are well documented elsewhere. The same holds true for the iterative determination of the aircraft center of gravity and wing sweep that provides a suitable level of longitudinal stability. However, there is one aspect of the basic planform that deserves some discussion; The wing taper ratio.

There are several factors to consider when selecting the wing taper ratio. Ref. 1 discusses a number of these problems, but methods in determining the proper taper ratio to avoid these pitfalls is limited. There are however two major considerations that we are able to deal with here that can be applied during the conceptual design phase. The

first of these considerations would be a method to determine the ideal taper ratio for minimum induced drag. The second consideration would be a method to determine an approximate taper ratio to avoid wing tip stall.

A. “Ideal” Taper Ratio

While there have been a number of discussions regarding the positive effect a bell shaped lift curve has on handling qualities, what if performance is a higher priority? It was noted in Ref. 2 that the spanwise location of the center of pressure is independent of aspect ratio for certain combinations of taper ratio and sweep angle, and that the resultant loading for these combinations was approximately elliptical. The resulting “ideal” taper ratios from Ref. 2 are plotted as a function of $\frac{1}{4}$ chord wing sweep in Fig. 2. It is readily apparent from Fig. 2 that the taper ratios decrease as the sweep angle is increased. This is to be expected since the increased upwash at the tips of a swept wing must be countered by a reduction of the local chord to keep the loading near elliptical. It is also important to note that these “ideal” taper ratios should require little to no twist to achieve minimum induced drag. Taper ratios below the “ideal” should not be selected since they will require negative wing twist (or wash-in) to compensate. It is difficult to arrive at any positive reason for adding wash-in to a tapered, swept wing configuration.

B. Longitudinal Stability Boundary

As described in Ref. 3, the nature of flow separation on swept wings usually occurs at the wing tip. Since this stall typically occurs behind the moment center, this may result in a nose-up, or unstable pitching moment variation. The initial work in empirically determining these boundaries was originally performed in Ref. 3 as a function of aspect ratio and wing sweep for untwisted, untapered wings. This work was further expanded and clarified in Ref. 4 to include the effect of taper ratio as well (though twist was still not taken into consideration). In short, it was determined in Ref. 4 that if the area behind the $\frac{1}{4}$ chord point of the mean aerodynamic chord (referred to as c') is greater than 69% of the total wing area, the wing is in a stable region. Likewise, if the area behind the $\frac{1}{4}$ chord point of c' falls below 69% of the total wing area, the wing is in an unstable region. The results from Ref. 3 and 4 may be seen in Fig. 3. Since the differences between the taper ratio curves is non-linear (and hence difficult to interpolate), the author has included the same figure with the inclusion of additional taper ratios in Fig. 4.

Since the phenomena causing the wing to cross into an unstable region is the wing tip stall, the author believes it is logical that the selection of values based upon Fig. 4 would help deter asymmetric wing tip stall as well. It's also important to remember that Fig. 4 does not include the effect of wing twist which, intuitively, should also help offset wing tip stall. While this probably shouldn't be taken into consideration during the conceptual design process without additional data, the addition of wash out to the configuration should provide some margin for those cases that may be borderline on Fig. 4.

C. Usage

In practice, while the conceptual designer is iterating on the basic planform he should be checking the selected taper ratio against Fig. 2 and 4 to try and stay as close to the “ideal” taper ratio as possible without crossing into the unstable region. In many cases the two will not agree, and the selected aspect ratio and sweep combination will result in higher taper ratios per Fig. 4 than what is considered “ideal” in Fig. 2. However, this eventuality will lead to the addition of wing twist (to be addressed in Section IV) to again achieve a minimum induced drag configuration, albeit for a single design point (e.g. cruise).

IV. Wing Twist for Minimum Induced Drag

It would be nice if the “ideal” taper ratio found in Fig. 2 always fell in the stable region of Fig. 4. As discussed previously, that is not always the case. So how does one regain the benefits of a minimum induced drag configuration for a straight tapered planform? As mentioned in Section I, after a great deal of searching the author stumbled upon an answer to this question in Ref. 5 while working on an unrelated problem. One of the methods for calculating the induced drag of straight tapered wings may be found in Section 4.1.5.2 of Ref. 5:

$$C_{DL} = \frac{C_L^2}{\pi A e} + C_L \theta c_{\ell \alpha} v + (\theta c_{\ell \alpha})^2 w \quad (1)$$

While looking at this equation and it's accompanying data, the author realized that all of the elements were there to identify the required twist to achieve a minimum induced drag configuration for a straight tapered planform. To

begin, we take the derivative of Eq. (1)* to obtain an equation for the slope of the induced drag curve. This would result in the following:

$$\frac{dC_{DL}}{d\theta} = C_L c_{\ell\alpha} v + 2\theta c_{\ell\alpha}^2 w \quad (2)$$

Setting the resulting equation for the slope equal to zero will yield a minima for Eq. (1):

$$0 = C_L c_{\ell\alpha} v + 2\theta c_{\ell\alpha}^2 w \quad (3)$$

If one manipulates Eq. (3) to isolate the wing twist, the resulting equation for the twist required to achieve minimum drag is:

$$\theta = -\frac{C_L v}{2c_{\ell\alpha} w} \quad (4)$$

As will become clear later, we introduce the compressibility factor β into Eq. 4, which yields:

$$\theta = -\frac{C_L}{2c_{\ell\alpha}} \left(\frac{v}{\beta w} \right) \beta \quad (5)$$

Per Ref. 5, using the value 2π per radian for $c_{\ell\alpha}$ is sufficiently accurate for this method. Therefore, Eq. 5 becomes:

$$\theta = -\frac{C_L}{4\pi} \left(\frac{v}{\beta w} \right) \beta \quad (radians) \quad (6)$$

Or:

$$\theta = -\frac{45C_L}{\pi^2} \left(\frac{v}{\beta w} \right) \beta \quad (degrees) \quad (7)$$

A review of Eq. (6) and Eq. (7) reveals that, per this method, the ideal twist of a tapered wing is a function of the wing lift coefficient, the ratio of $\frac{v}{\beta w}$, and the compressibility factor β . For convenience, the ratio $\frac{v}{\beta w}$ has been interpolated from the original data in Ref. 5, and replotted in Fig. 5 - 14[†].

V. Trim

Since the method being proposed does not use wing twist to achieve trim, this must be achieved by using airfoils with the correct (typically positive) pitching moments. As is commonly known, the value of the pitching moment coefficient for a wing is:

$$C_m = C_{m_0} + \frac{dC_m}{dC_L} C_L \quad (8)$$

Since we desire for our aircraft to be trimmed, the pitching moment coefficient in Eq. (8) must equal zero. Therefore:

$$0 = C_{m_0} + \frac{dC_m}{dC_L} C_L \quad (9)$$

If we then rearrange to isolate the zero lift pitching moment, we find that:

* According to Ref. 5, Eq. 1 and all of its supporting data were taken from Lundry, J., "Charts for Obtaining Subsonic Inviscid Induced Drag of Twisted Swept Wings," Douglas Aircraft Company, Report LB-31689, 1964. The author would be interested in obtaining a copy of this report if one is found.

[†] For completeness, the original plots for v and βw from Ref. 5 have been included in Fig. 26 – 34, and Fig. 35 – 43 respectively.

$$C_{m_0} = -\frac{dC_m}{dC_L} C_L \quad (10)$$

The wing zero lift pitching moment (C_{m_0}) required to trim the aircraft may be easily calculated since the static margin $\left(\frac{dC_m}{dC_L}\right)^\dagger$ should have been determined during the initial planform analysis discussed in Section III, and the lift coefficient (C_L) already selected for our design point. If we then refer to Section 4.1.4.1 of Ref. 5 we also find that for wings with linear twist, the zero lift pitching moment must also equal:

$$C_{m_0} = \left((C_{m_0})_{\theta=0} + \left(\frac{\Delta C_{m_0}}{\theta}\right)\theta \right) \gamma \quad (11)$$

Where θ is in degrees from Eq. 7, and $\frac{\Delta C_{m_0}}{\theta}$ may be found in Fig. 15 - 24[§]. The factor γ is the compressibility correction factor to the wing zero-lift pitching moment coefficient from Ref. 5:

$$\gamma = \frac{(C_{m_0})_M}{(C_{m_0})_{M=0}} \quad (12)$$

If compressibility is an issue, the factor $\frac{(C_{m_0})_M}{(C_{m_0})_{M=0}}$ is presented in Fig. 25^{**} which was also obtained from Ref. 5. Lastly, per Section 4.1.4.1 of Ref. 5 we also find:

$$(C_{m_0})_{\theta=0} = \frac{A \cos^2 \Lambda_{c/4}}{A + 2 \cos \Lambda_{c/4}} \left(\frac{c_{m_{0root}} + c_{m_{0tip}}}{2} \right) \quad (13)$$

If we substitute Eq. (13) into Eq. (11) we arrive at the wing zero lift pitching moment equaling:

$$C_{m_0} = \left(\frac{A \cos^2 \Lambda_{c/4}}{A + 2 \cos \Lambda_{c/4}} \left(\frac{c_{m_{0root}} + c_{m_{0tip}}}{2} \right) + \left(\frac{\Delta C_{m_0}}{\theta}\right)\theta \right) \gamma \quad (14)$$

If we then rearrange Eq. (14) to isolate the airfoil zero lift pitching moment terms, we find:

$$\left(\frac{c_{m_{0root}} + c_{m_{0tip}}}{2} \right) = \left(\frac{C_{m_0}}{\gamma} - \left(\frac{\Delta C_{m_0}}{\theta}\right)\theta \right) \frac{A + 2 \cos \Lambda_{c/4}}{A \cos^2 \Lambda_{c/4}} \quad (15)$$

Substituting Eq. (10), the airfoil zero lift pitching moments required for trim are then found to be:

$$\boxed{\left(\frac{c_{m_{0root}} + c_{m_{0tip}}}{2} \right) = \left(\frac{-\frac{dC_m}{dC_L} C_L}{\gamma} - \left(\frac{\Delta C_{m_0}}{\theta}\right)\theta \right) \frac{A + 2 \cos \Lambda_{c/4}}{A \cos^2 \Lambda_{c/4}}} \quad (16)$$

[†] If compressibility is a consideration, the effect on $\frac{dC_m}{dC_L}$ should be accounted for using an appropriate method such as that found in Ref. 5, Section 4.1.4.2.

[§] Fig. 15 - 24 were replotted by the author to be consistent with the aspect ratios presented in Fig. 5 - 14. This required some extrapolation since the maximum aspect ratio was 10 in the original plots from Ref. 5. Ref. 5 also states that this method should be used for cases where $\Lambda_{c/4} < 45^\circ$. While the resulting plots in Fig. 15 - 24 look reasonable, caution should be used when using these plots above $A = 10$ and $\Lambda_{c/4} \geq 45^\circ$. As before, the original plots for $\frac{\Delta C_{m_0}}{\theta}$ have been included in Fig. 44 - 46 for completeness.

^{**} The factor γ does not appear in Ref. 5, but was inserted by the author to simplify the writing of these equations.

If airfoils with identical zero lift pitching moments are desired, Eq. (16) may be simplified to:

$$c_{m_0} = \left(\frac{-\frac{dc_m}{dc_L} c_L}{\gamma} - \left(\frac{\Delta c_{m_0}}{\theta} \right) \theta \right) \frac{A + 2 \cos \Lambda_{c/4}}{A \cos^2 \Lambda_{c/4}} \quad (17)$$

The airfoil zero lift pitching moments obtained from Eq. (16) or (17) may then be used in the selection or design^{††} of airfoils that trim the configuration developed from Sections III and IV above.

VI. Conclusion

As discussed in Section III, methods have been provided in Fig. 2 and 4 to help guide the conceptual designer in the selection of taper ratios that are close to ideal, while also helping to mitigate negative tip up and wing tip stall behavior. A method for calculating the wing twist required to achieve a minimum induced drag configuration is also included in Eq. (6) and (7). Finally, the airfoil pitching moments required to trim the resulting configuration may be calculated using Eq. (16) or (17). The resulting airfoil pitching moments may then be used in the selection or design of adequate airfoils to support the calculated requirements.

Since better tools exist in the major design houses, it's assumed that a majority of conceptual designers using these methods would be homebuilt aircraft enthusiasts or modellers. Therefore, one area for future work on the methods discussed in Sections IV and V would involve expanding the plots to add aspect ratios above the current 10/14 limit to support the conceptual design of flying wing sailplanes. Due to the number of data points required, this work would require the automation of a vortex lattice model to run all of the data points in quick succession. The new values of v , w and $\frac{\Delta c_{m_0}}{\theta}$ may then be easily calculated, and new plots generated.

Appendix

For those curious about the Crossbow configuration, the basic design requirement was to develop a theoretical follow-on to the Ex-Drone delta-wing, tractor configuration that was in use with the Marine Corps at the time. Since the Ex-Drone was either rocket or bungee/dolly launched, the aircraft did not have landing gear. Instead it included a skid arrangement for recovery. The student designs followed this pattern, and all Crossbow launches were performed using a dolly and two bungees.

Crossbow had a cranked wing that was a legacy of the initial design layouts when the team was trying to arrive at the correct aerodynamic center and center-of-gravity positions. It could have been abandoned later in the design process, but the team rejected the change due to time constraints. This probably wasn't all bad since the cranked wing made the lofting into the payload section of the fuselage a bit easier. The dihedral in the wing tips so readily apparent in Figure 1 was the result of the VSAERO model predictions that this would have a slightly positive impact to lateral direction stability. Controls included a set of elevons inboard, and split drag rudders outboard. The split drag rudders were connected to a common rate gyro of the type available to Radio Control enthusiasts at the time (circa 1990). The vertical plates on the wingtips were removable, and three different sizes were made so the team could slowly work down to a no-vertical configuration during flight testing.

A total of five flights were made on the Crossbow (note the black silhouettes denoting each flight painted onto to port orange stripe). Due to time constraints during flight testing, the teams plan to work down in vertical plate sizes was abandoned, and a single flight was made without verticals. During a slow, high pass the aircraft encountered what appeared to be a severe wing rock. The pilot added power in an attempt to recover, but the aircraft began a slow diving spiral to the right, rolling severely both directions the entire time (probably best described as wing rock). The pilot was finally able to recover when the aircraft had regained enough airspeed that it finally stabilized.

In hindsight, the wing rock was probably a combination of factors. First, it is possible that the dihedral added to the tips based upon the VSAERO model results potentially placed the aircraft over the lateral stability boundary at low speeds. A team with more experience would probably have realized that adding more dihedral should not have had a positive effect, and that the limits of accuracy of the VSAERO model were probably encountered. Second, the team had not made allowances for the potential rolling moment imparted by a symmetric deflection of the upper and lower surface split drag rudders, especially at low speeds. Lastly, the team had no way of estimating the proper gain

^{††} While the design of airfoils may seem daunting, initial approximations of suitable airfoils may be achieved using additive mean lines and thickness distributions as discussed in Section 6.10 of Ref. 6. These initial approximations may then be used in an airfoil design program such as XFOIL to finalize the design.

setting for the rate gyro on the split drag rudders. The author believes the severe wing rock was most likely caused by the rate gyro deflecting the split drag rudders in response to a (from the ground) nearly imperceptible yaw component of the dutch roll mode. The corresponding rolling moment imparted by the symmetric deflections of the split drag rudders then amplified the roll component of that mode. The wing rock imparted by this combination of factors only subsided when the aircraft developed enough airspeed that the aircraft passed outside of the region of low yaw stability.

References

- ¹Karl Nickel and Michael Wohfahrt, *Tailless Aircraft in Theory and Practice*, AIAA, Washington, 1994
- ²DeYoung, John, and Harper George W., "Theoretical Symmetric Span Loading at Subsonic Speeds for Wings Having Arbitrary Plan Form," NACA Technical Report 921, 1948
- ³Shortal, Joseph A., and Maggin, Bernard, "Effect of Sweepback and Aspect Ratio on Longitudinal Stability Characteristics of Wings at Low Speeds," NACA TN 1093, 1946
- ⁴Furlong, G. Chester, and McHugh, James G., "A Summary and Analysis of the Low-Speed Longitudinal Characteristics of Swept Wings at High Reynolds Number," NACA Technical Report 1339, 1957
- ⁵Finck, R. D., "USAF Stability and Control DATCOM," USAF Technical Report AFWAL-TR-83-3048, April 1978
- ⁶Abbot, Ira H., and Doenhoff, Albert E., *Theory of Wing Sections*, Dover Publications, New York, 1959

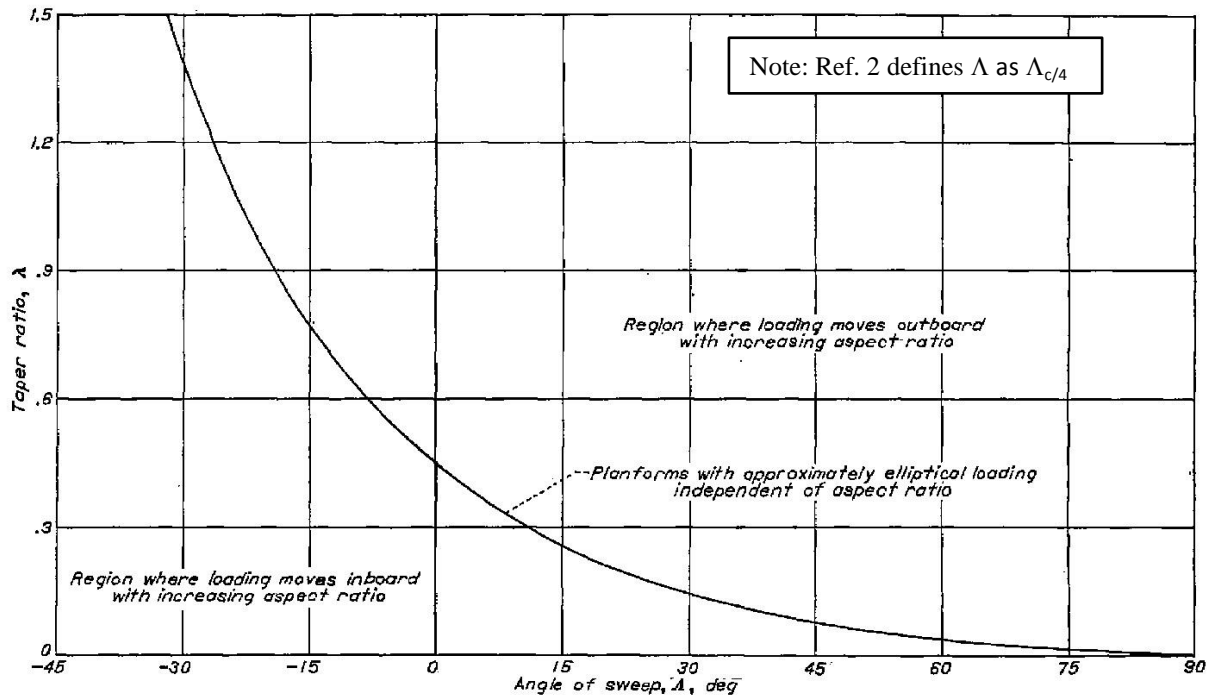


Figure 2 - Taper Ratio Required for Aproximate Elliptical Loading (Ref. 2)

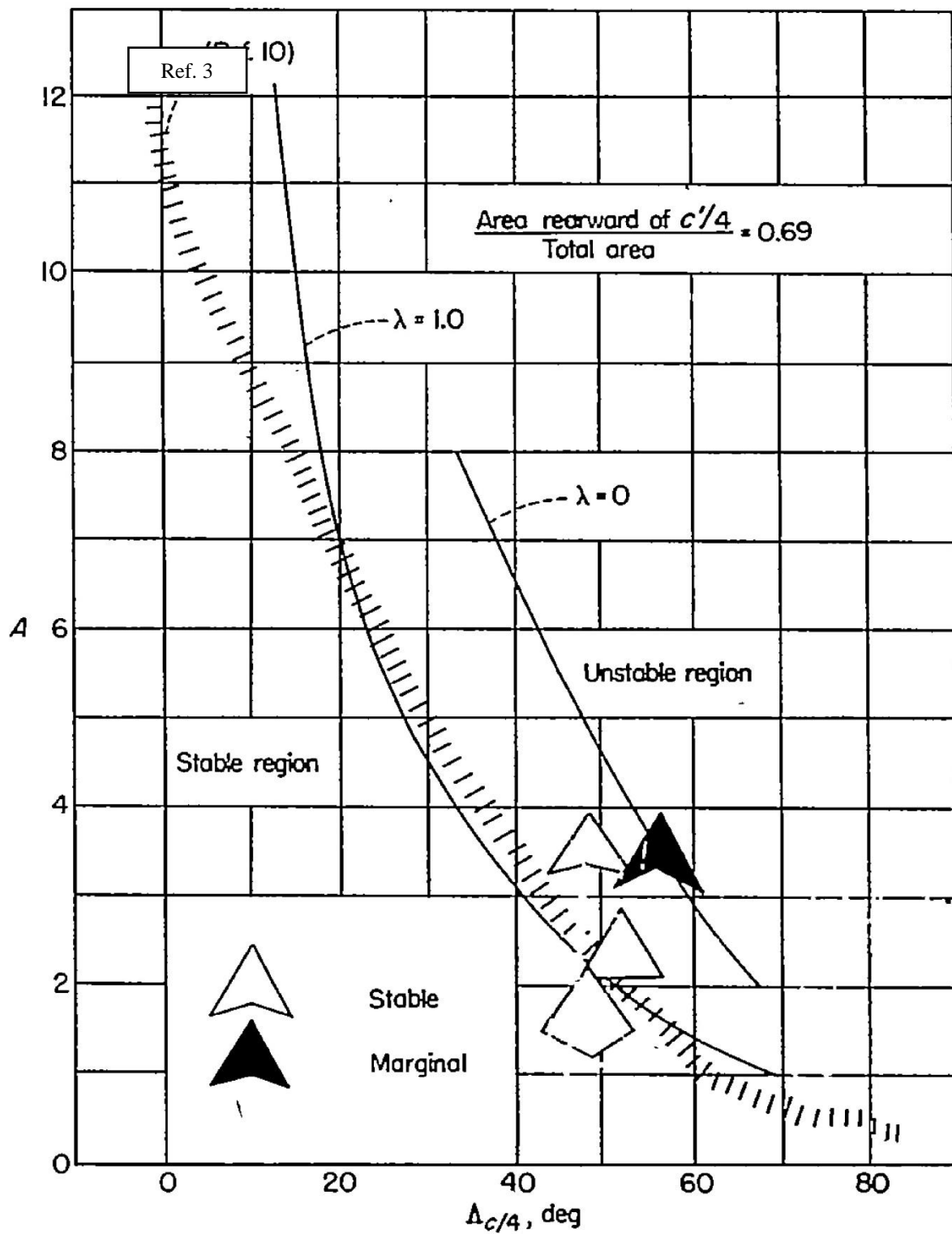


Figure 3- Empirical Longitudinal-Stability Boundary (Ref. 4)

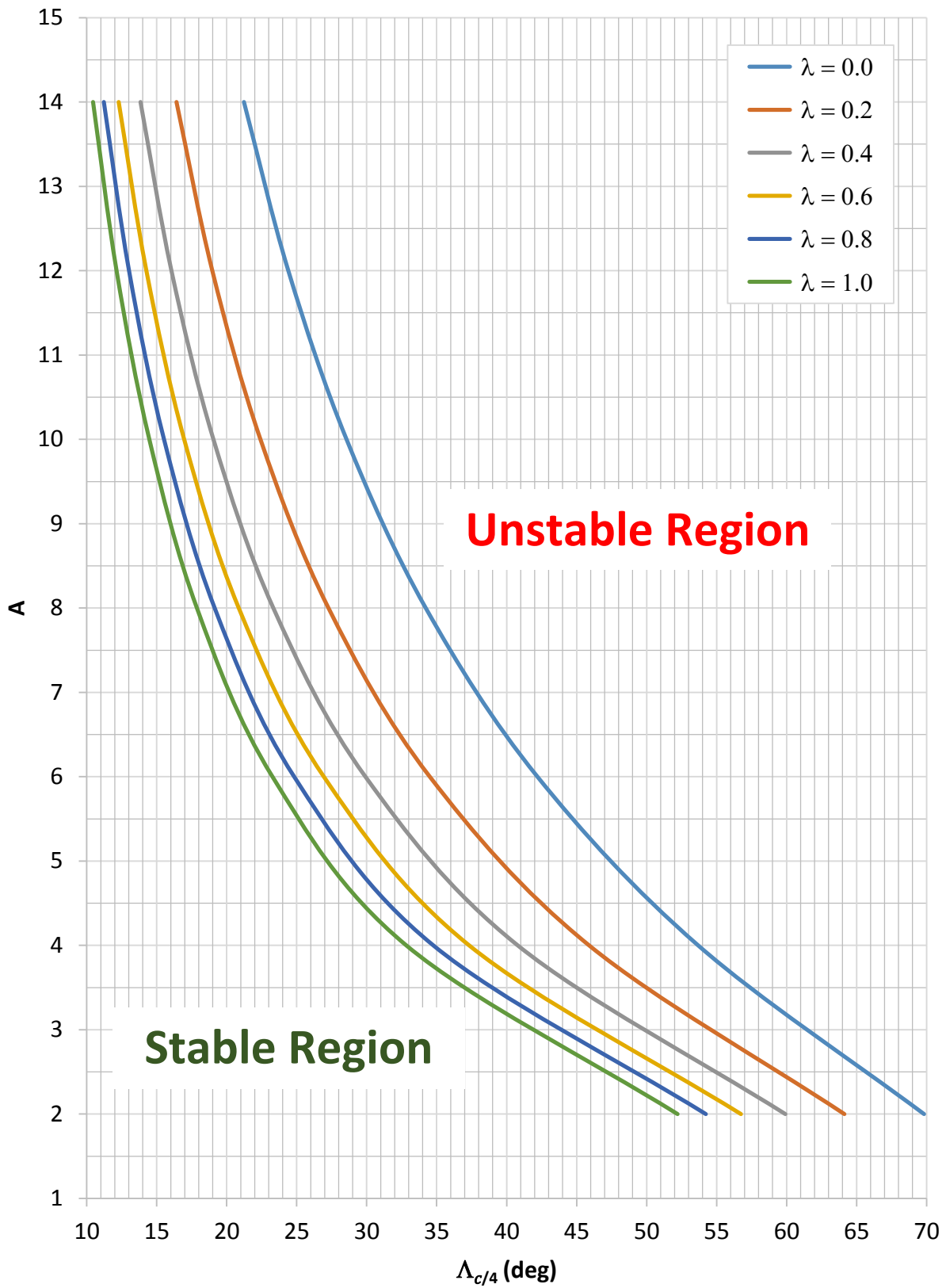


Figure 4 - Empirical Longitudinal-Stability Boundary

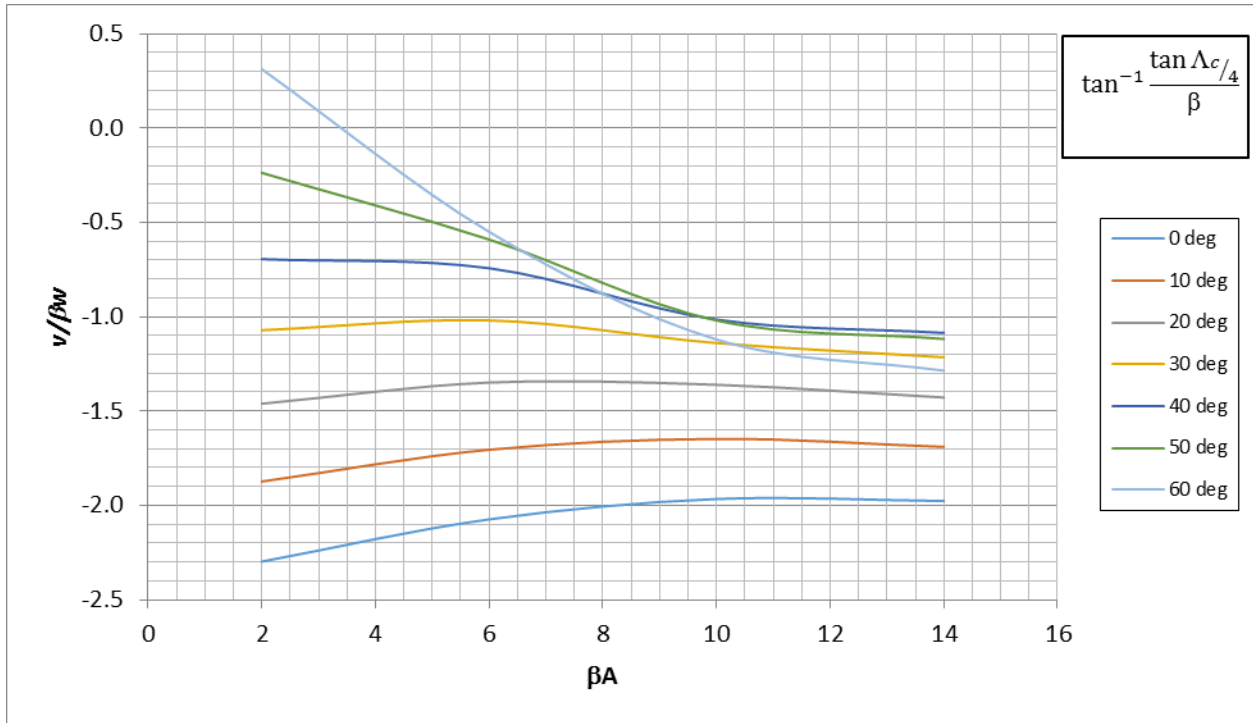


Figure 5 - Ratio of lift dependent and zero lift drag factors ($v/\beta w$), ($\lambda=0.1$)

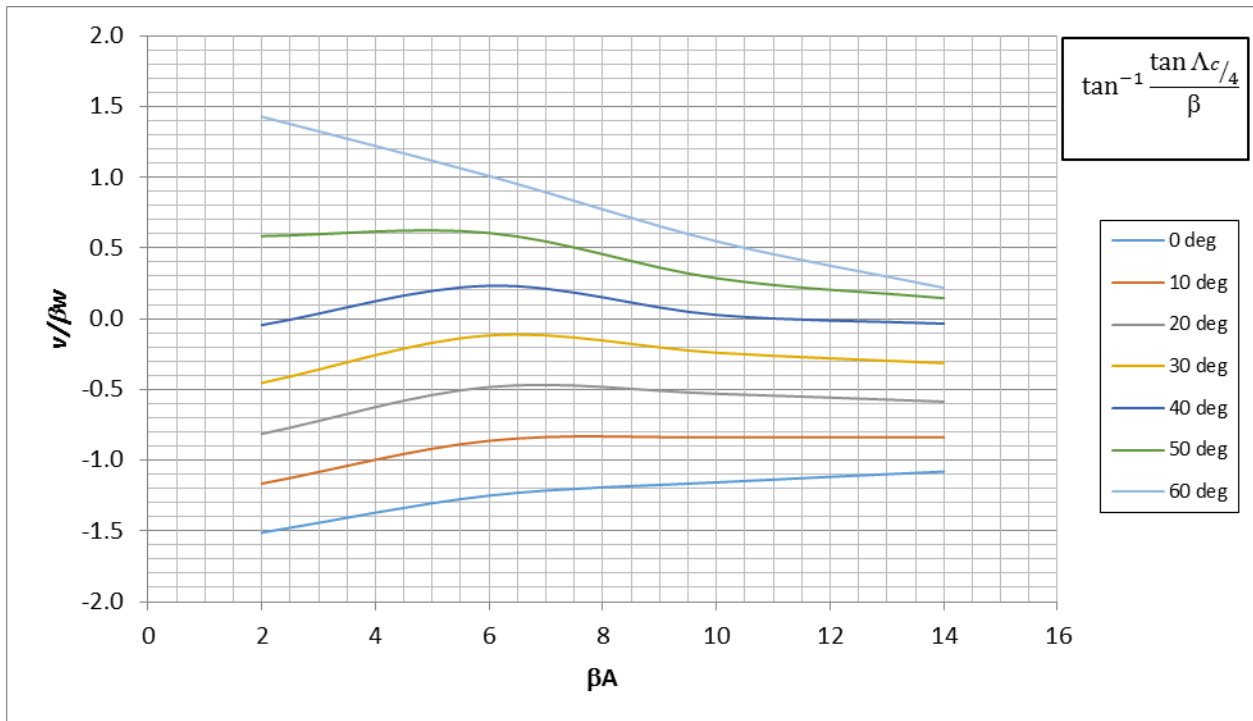


Figure 6 - Ratio of lift dependent and zero lift drag factors ($v/\beta w$), ($\lambda=0.2$)

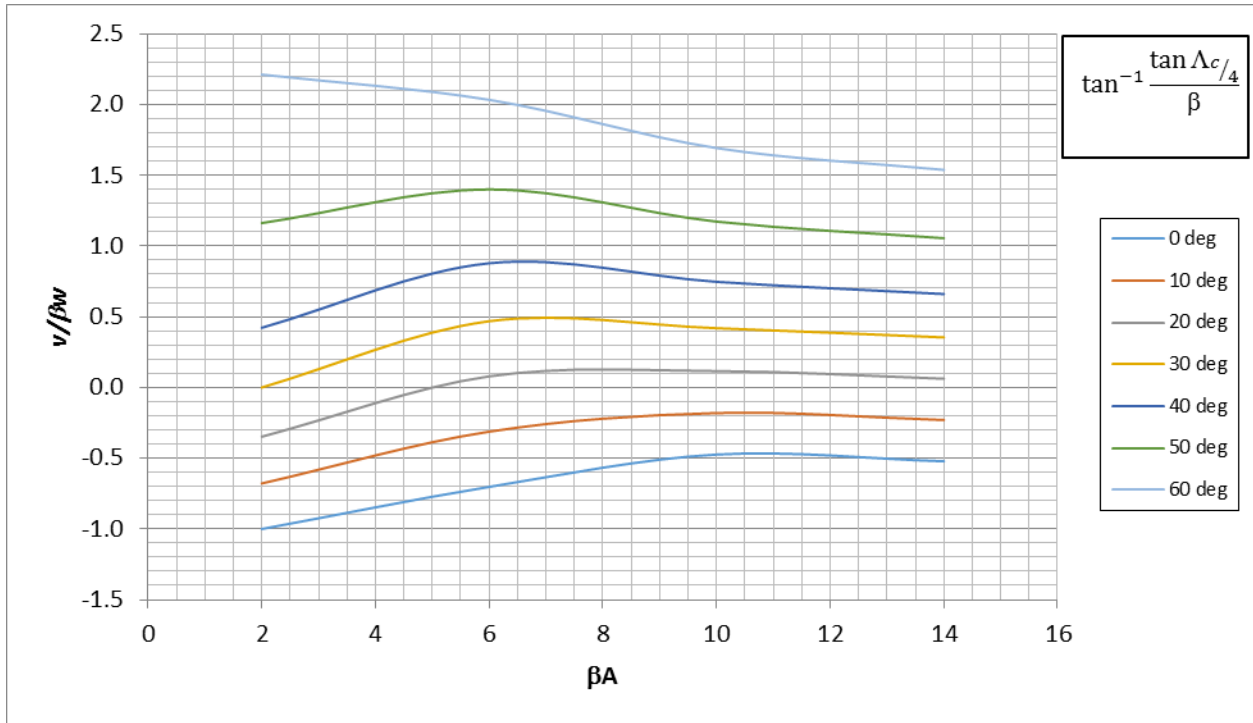


Figure 7 - Ratio of lift dependent and zero lift drag factors ($v/\beta w$), ($\lambda=0.3$)

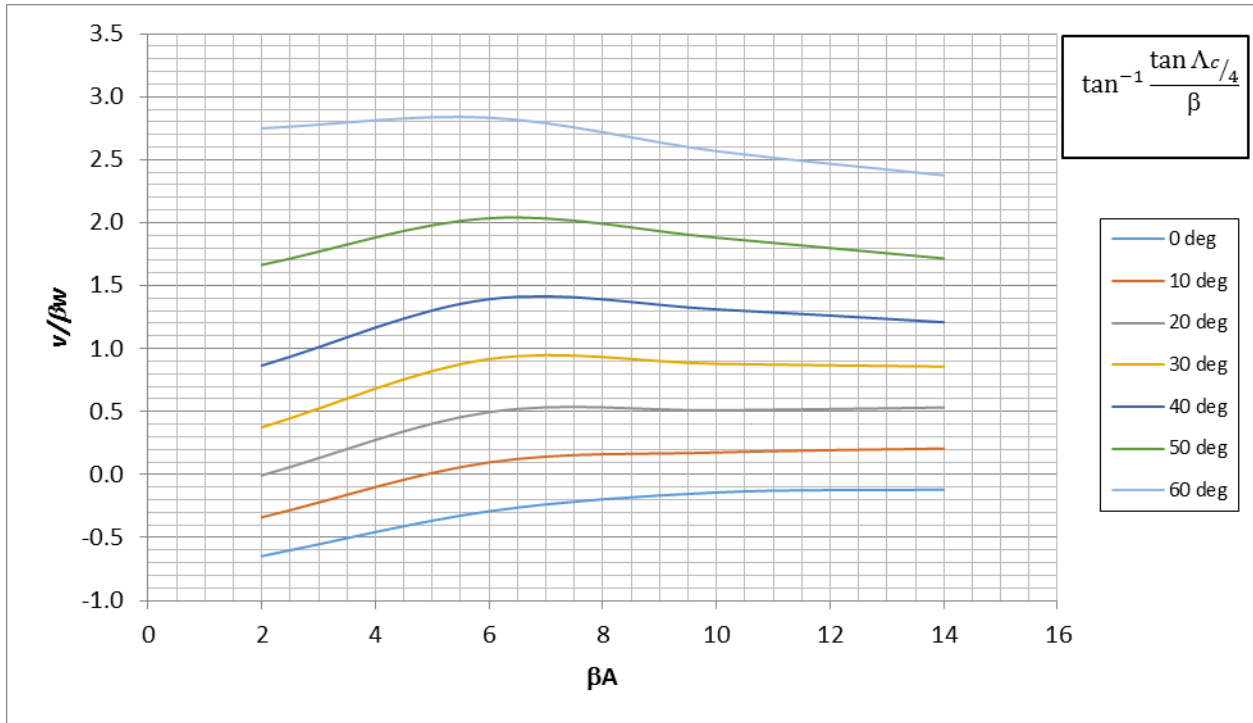


Figure 8 - Ratio of lift dependent and zero lift drag factors ($v/\beta w$), ($\lambda=0.4$)

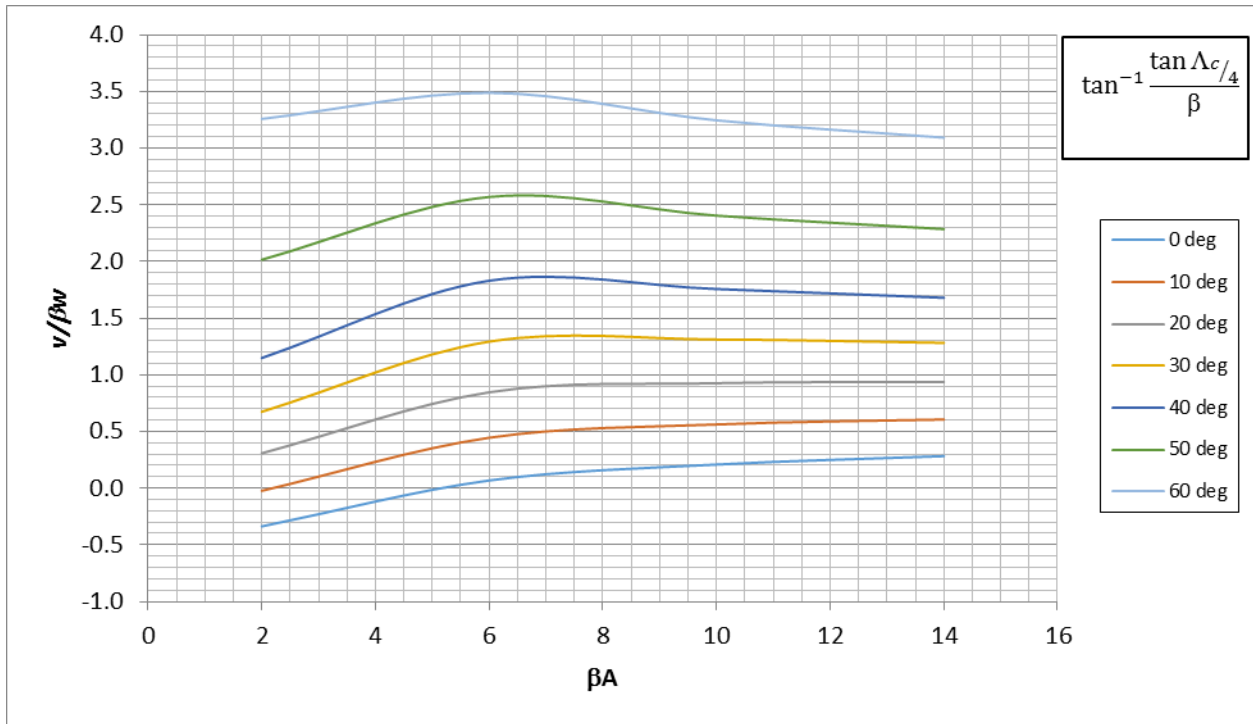


Figure 9 - Ratio of lift dependent and zero lift drag factors ($v/\beta w$), ($\lambda=0.5$)

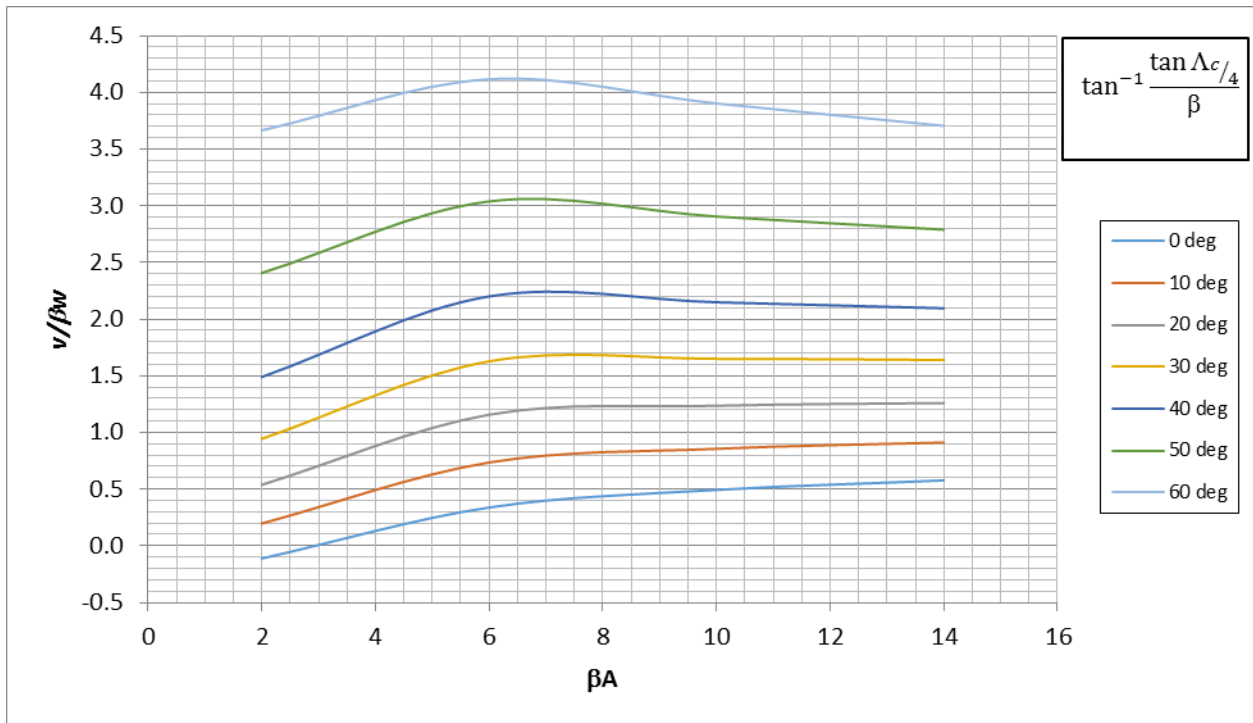


Figure 10 - Ratio of lift dependent and zero lift drag factors ($v/\beta w$), ($\lambda=0.6$)

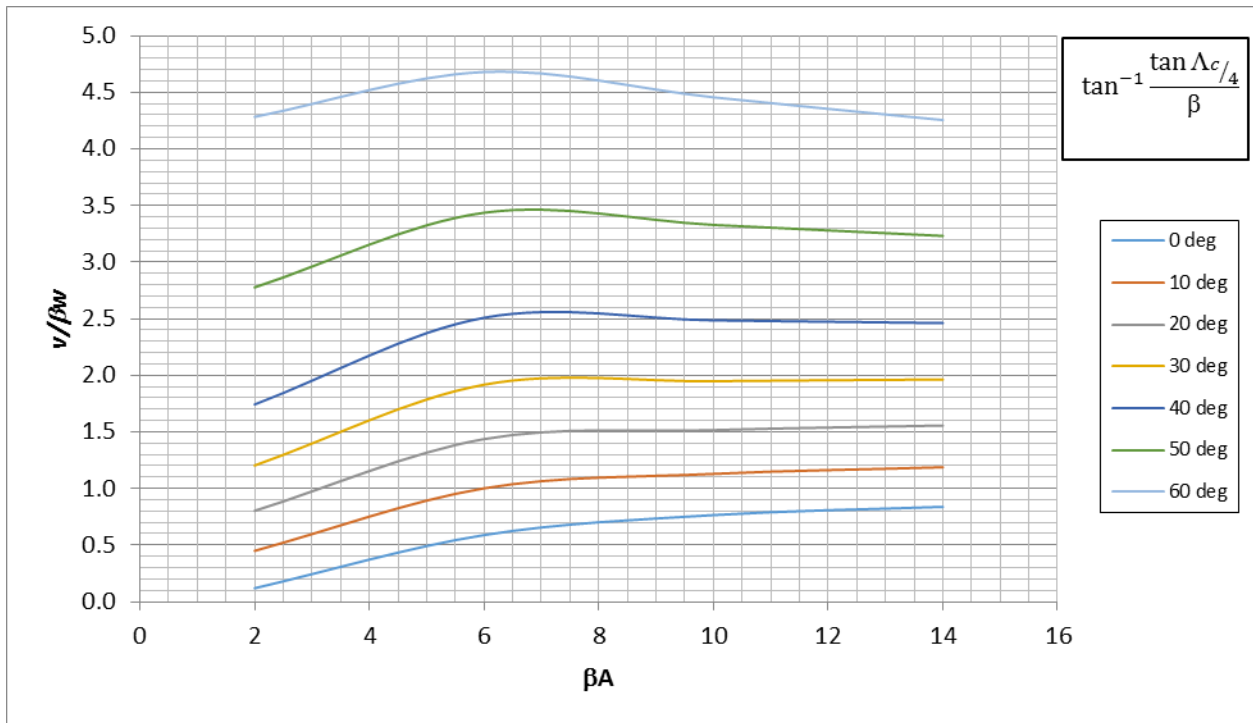


Figure 11 - Ratio of lift dependent and zero lift drag factors ($v/\beta w$), ($\lambda=0.7$)

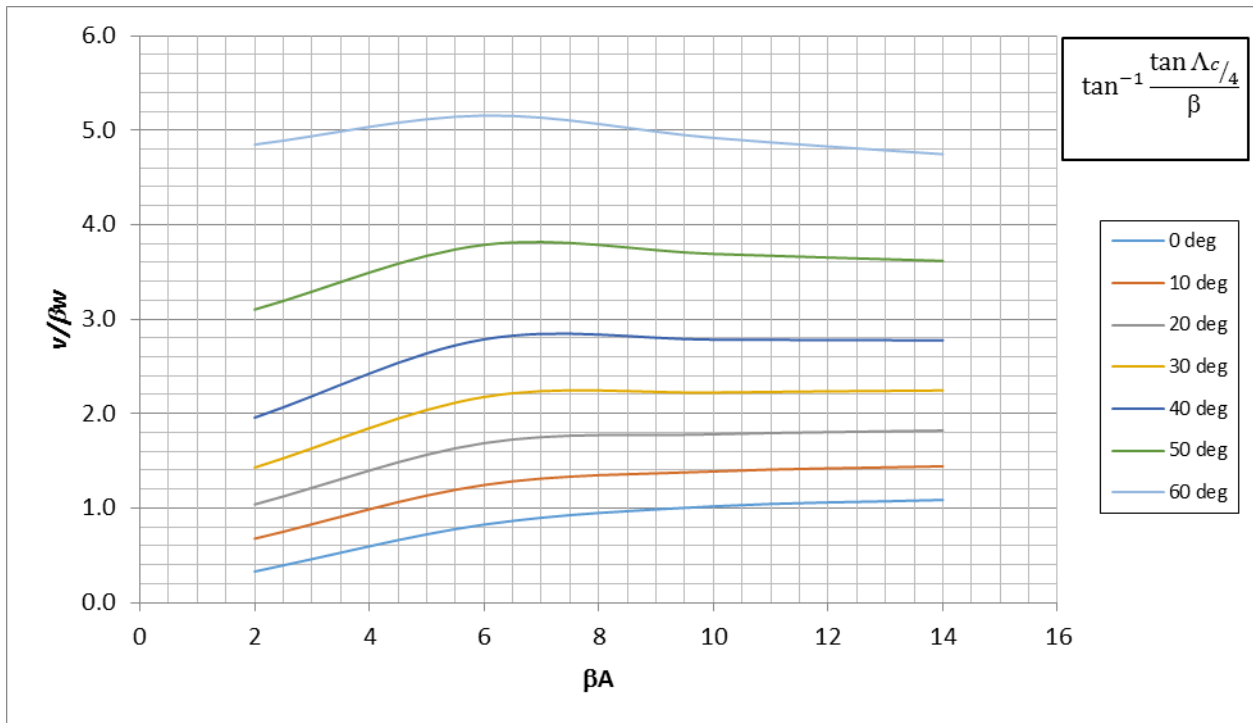


Figure 12 - Ratio of lift dependent and zero lift drag factors ($v/\beta w$), ($\lambda=0.8$)

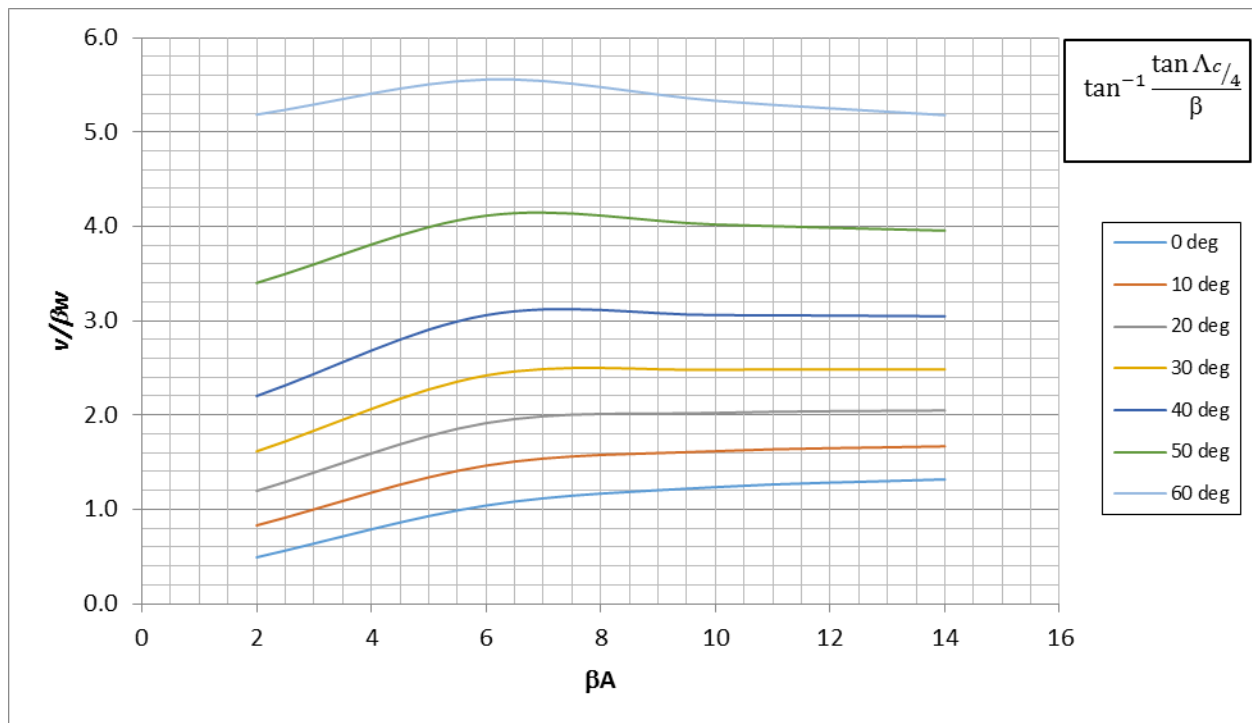


Figure 13 - Ratio of lift dependent and zero lift drag factors ($v/\beta w$), ($\lambda=0.9$)

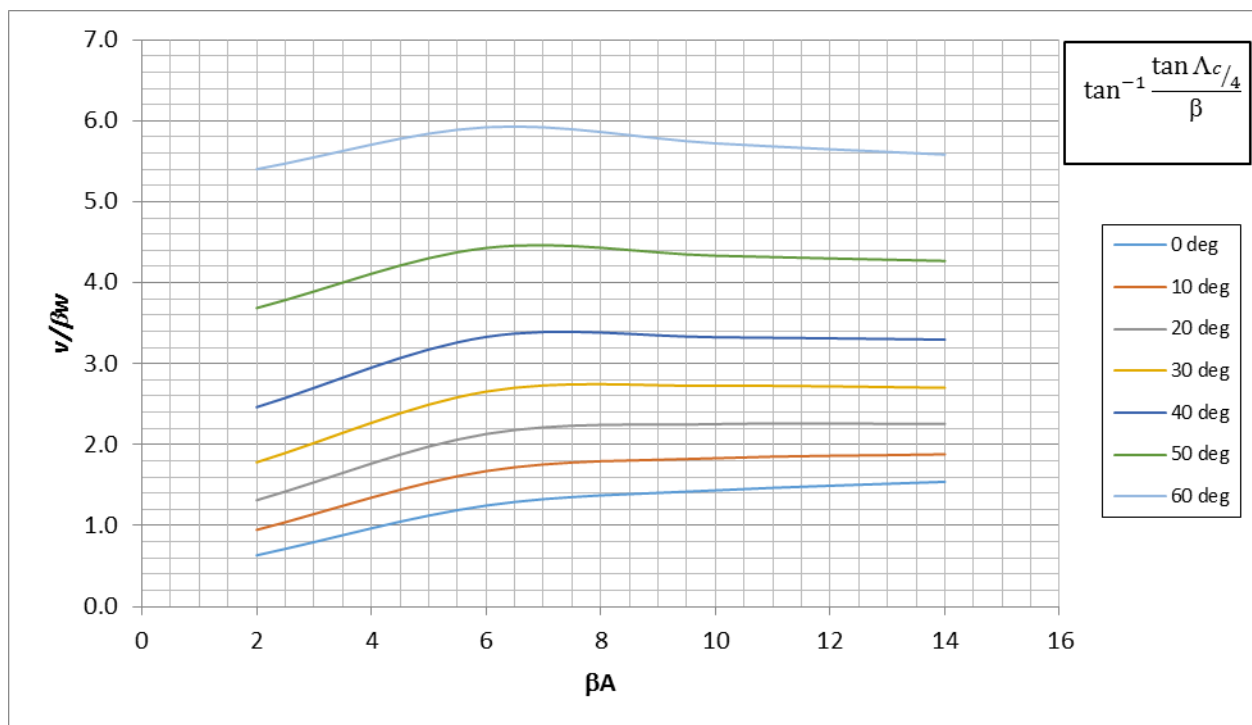


Figure 14 - Ratio of lift dependent and zero lift drag factors ($v/\beta w$), ($\lambda=1.0$)

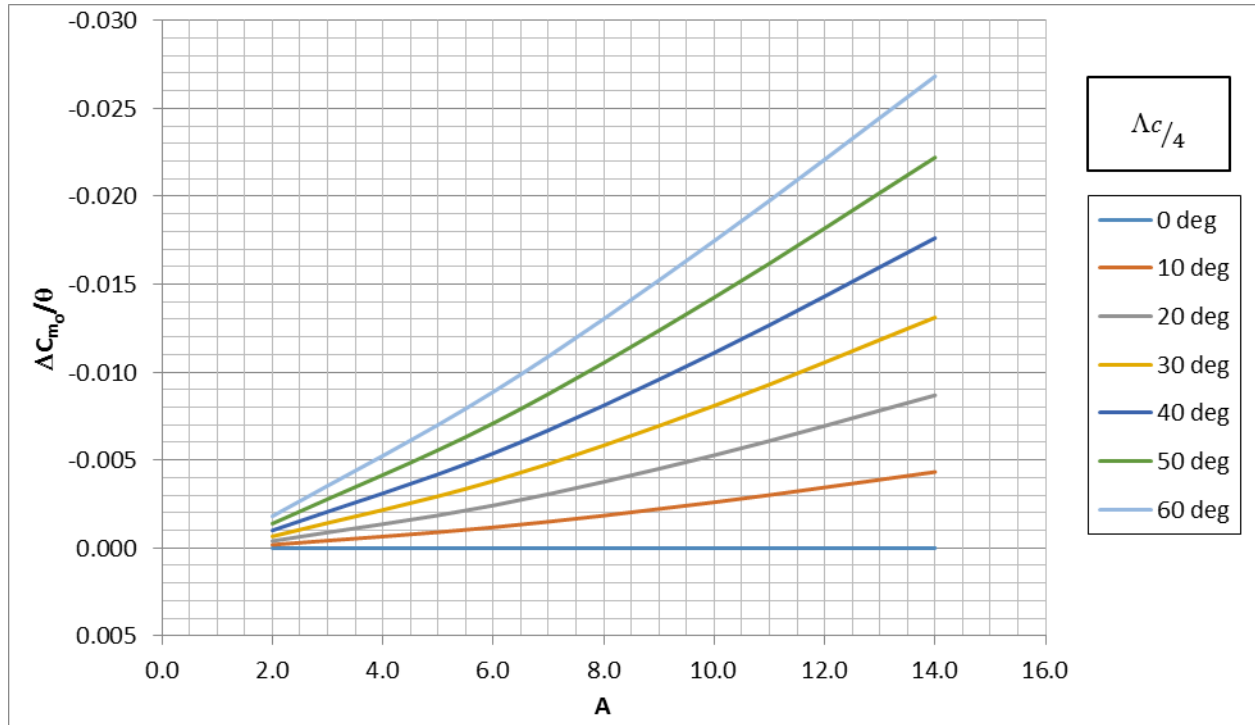


Figure 15 - Effect of Linear Twist on the Wing Zero-Lift Pitching Moment, ($\lambda=0.1$)

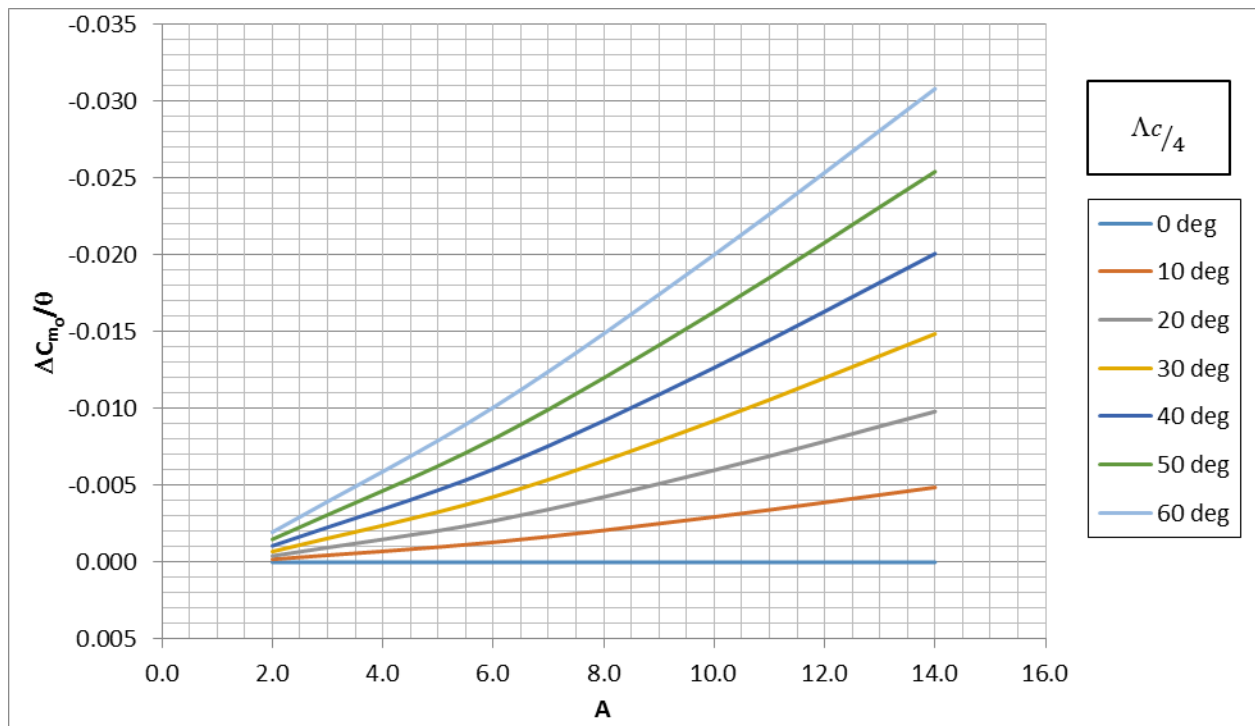


Figure 16 - Effect of Linear Twist on the Wing Zero-Lift Pitching Moment, ($\lambda=0.2$)

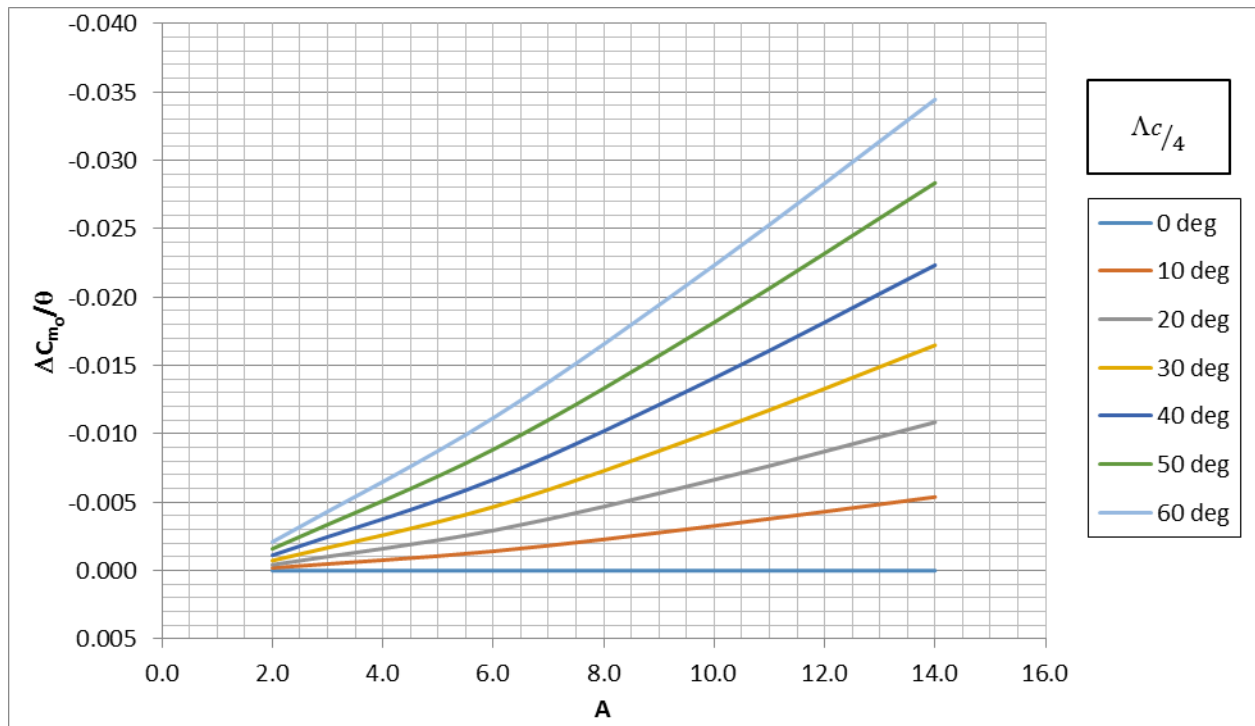


Figure 17 - Effect of Linear Twist on the Wing Zero-Lift Pitching Moment, ($\lambda=0.3$)

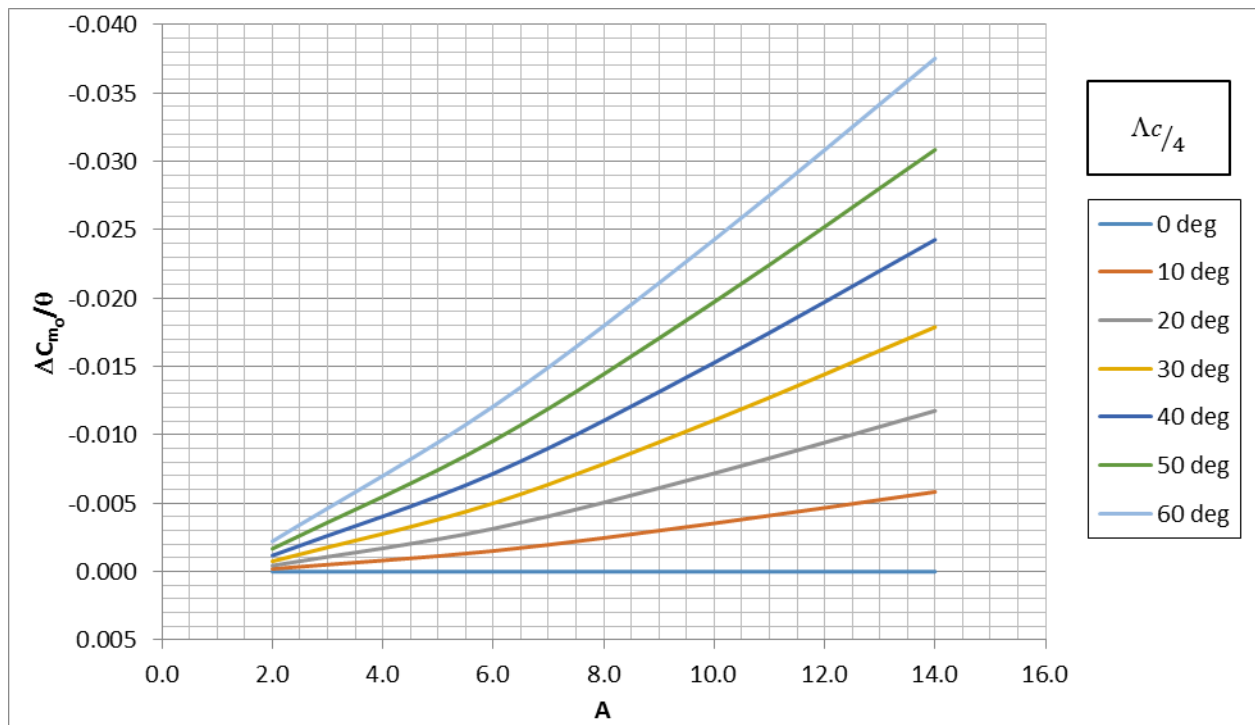


Figure 18 - Effect of Linear Twist on the Wing Zero-Lift Pitching Moment, ($\lambda=0.4$)

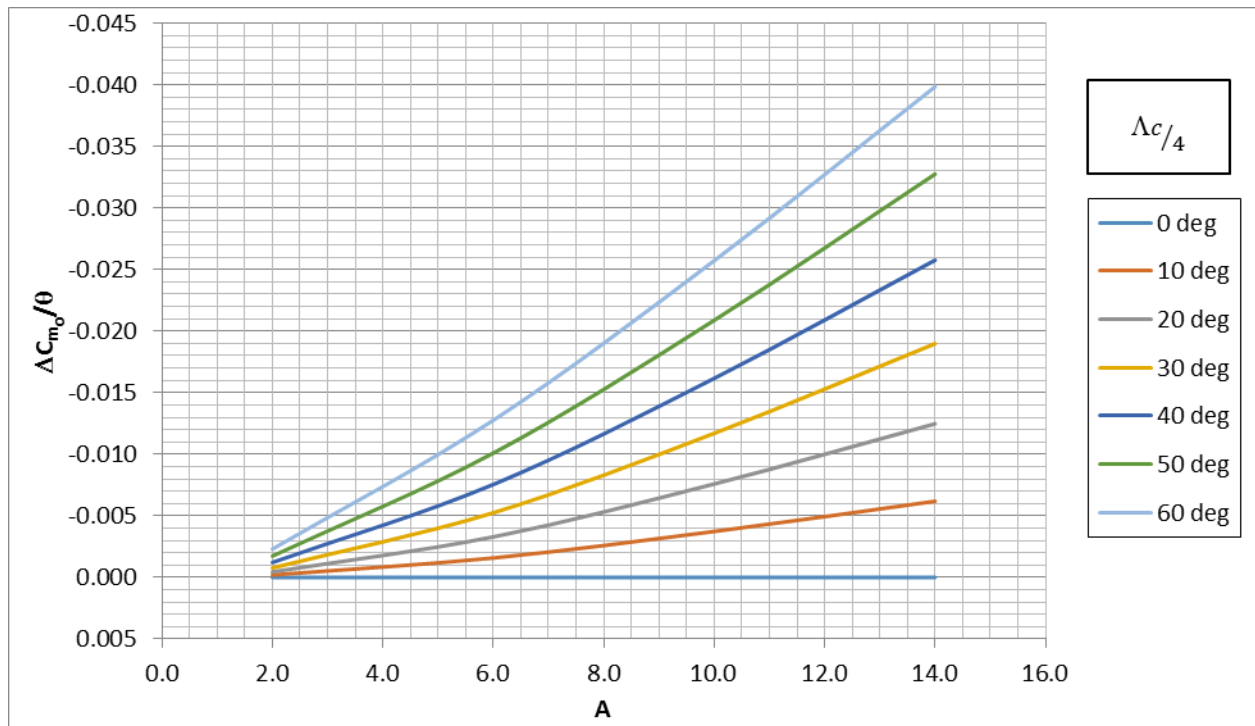


Figure 19 - Effect of Linear Twist on the Wing Zero-Lift Pitching Moment, ($\lambda=0.5$)

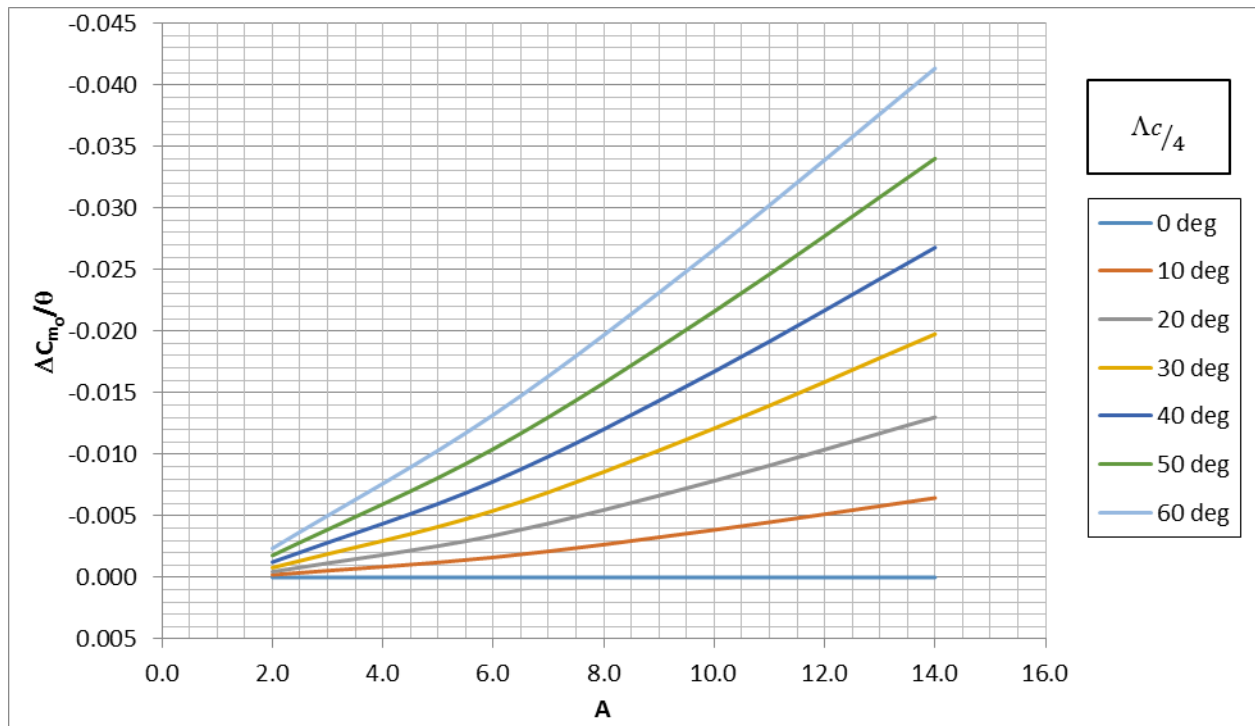


Figure 20 - Effect of Linear Twist on the Wing Zero-Lift Pitching Moment, ($\lambda=0.6$)

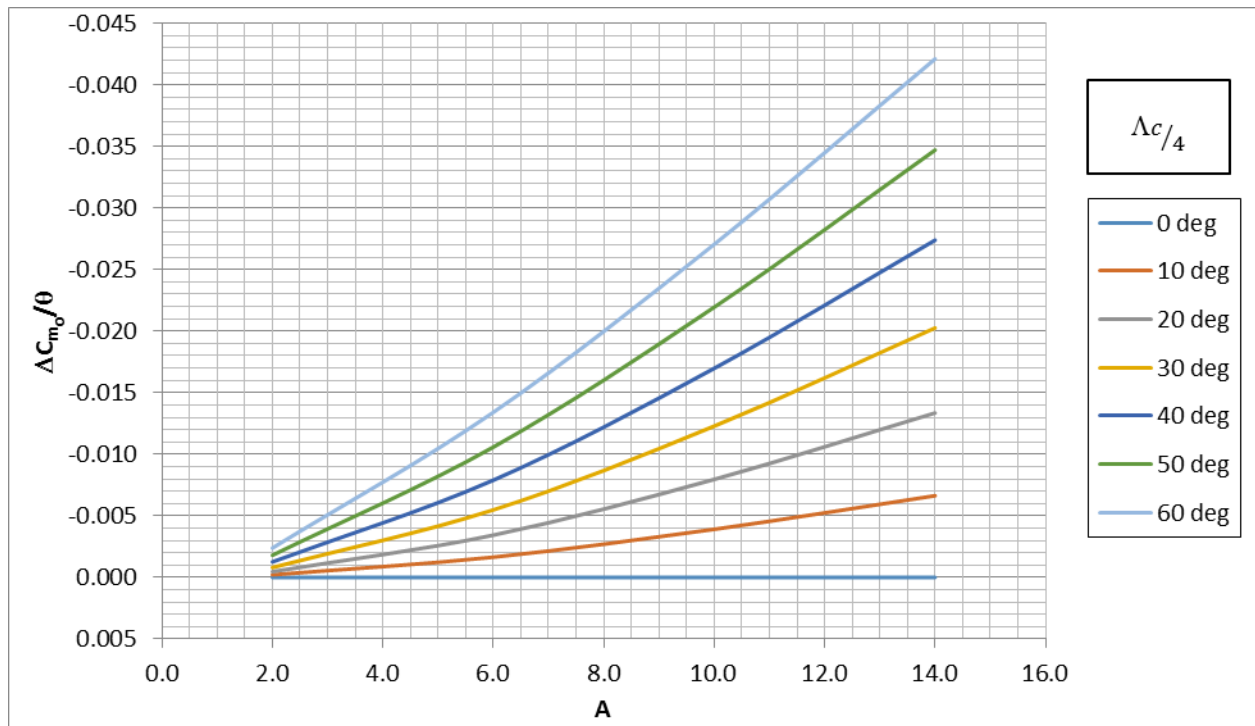


Figure 21 - Effect of Linear Twist on the Wing Zero-Lift Pitching Moment, ($\lambda=0.7$)

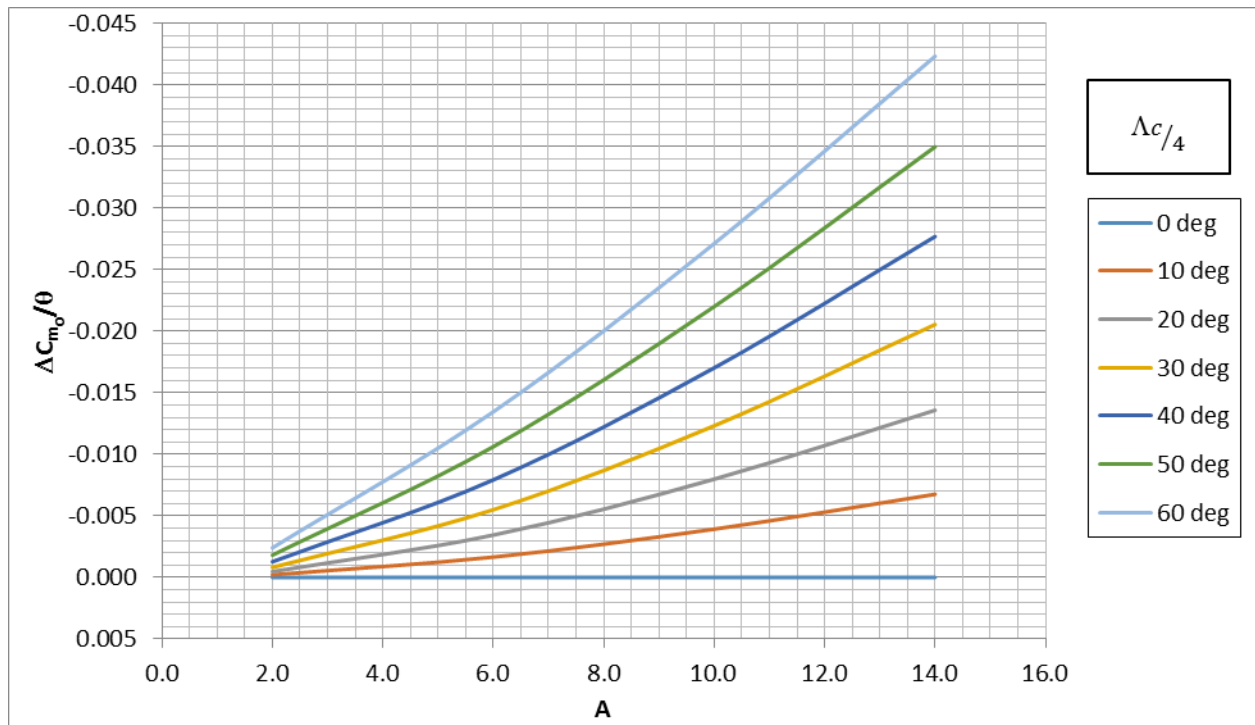


Figure 22 - Effect of Linear Twist on the Wing Zero-Lift Pitching Moment, ($\lambda=0.8$)

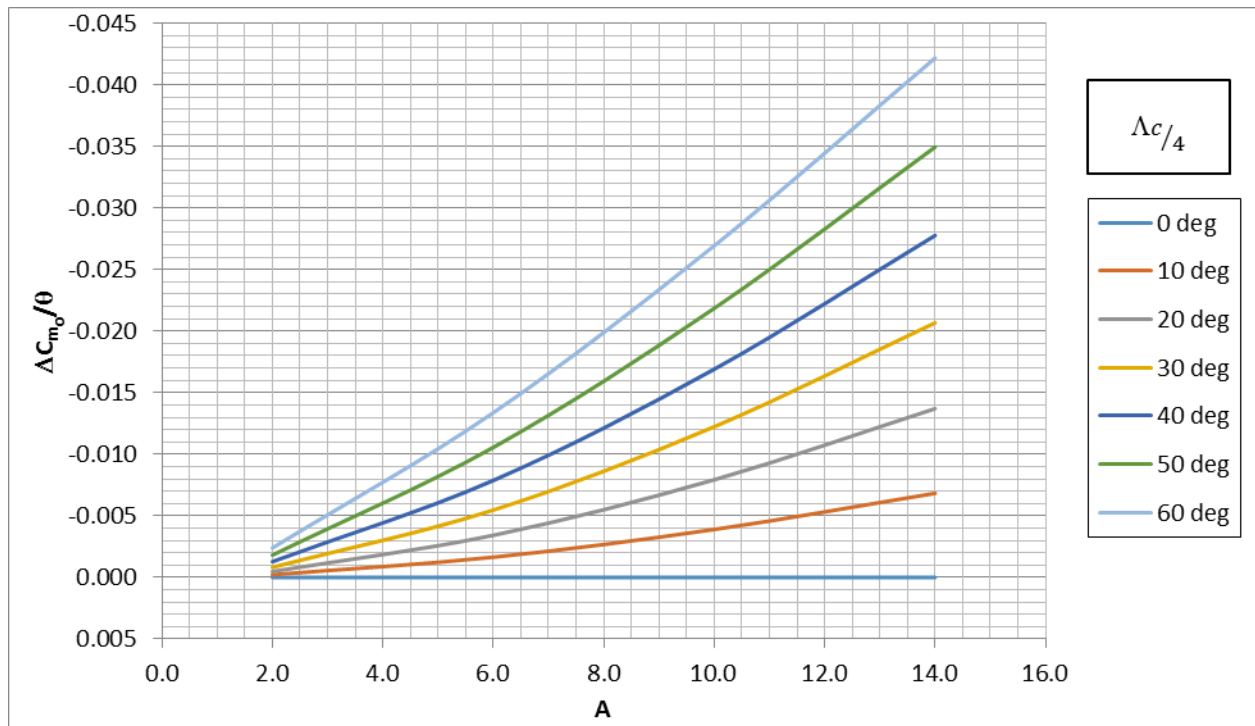


Figure 23 - Effect of Linear Twist on the Wing Zero-Lift Pitching Moment, ($\lambda=0.9$)

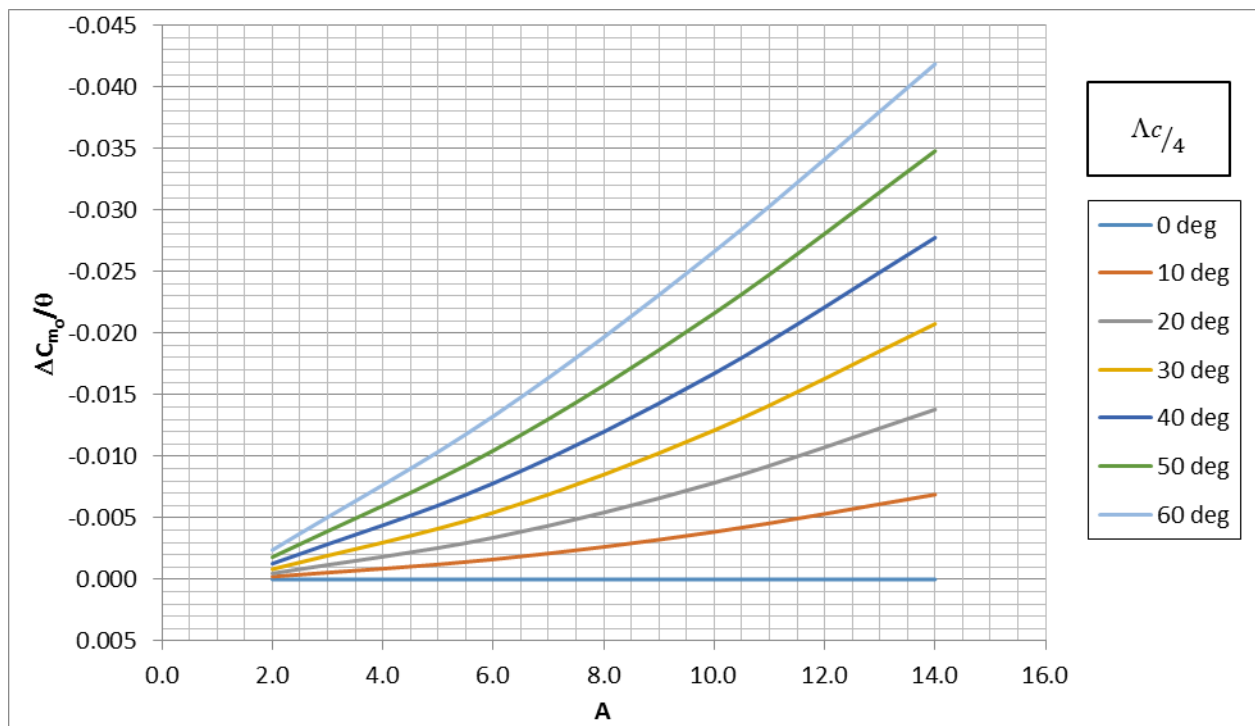


Figure 24 - Effect of Linear Twist on the Wing Zero-Lift Pitching Moment, ($\lambda=1.0$)

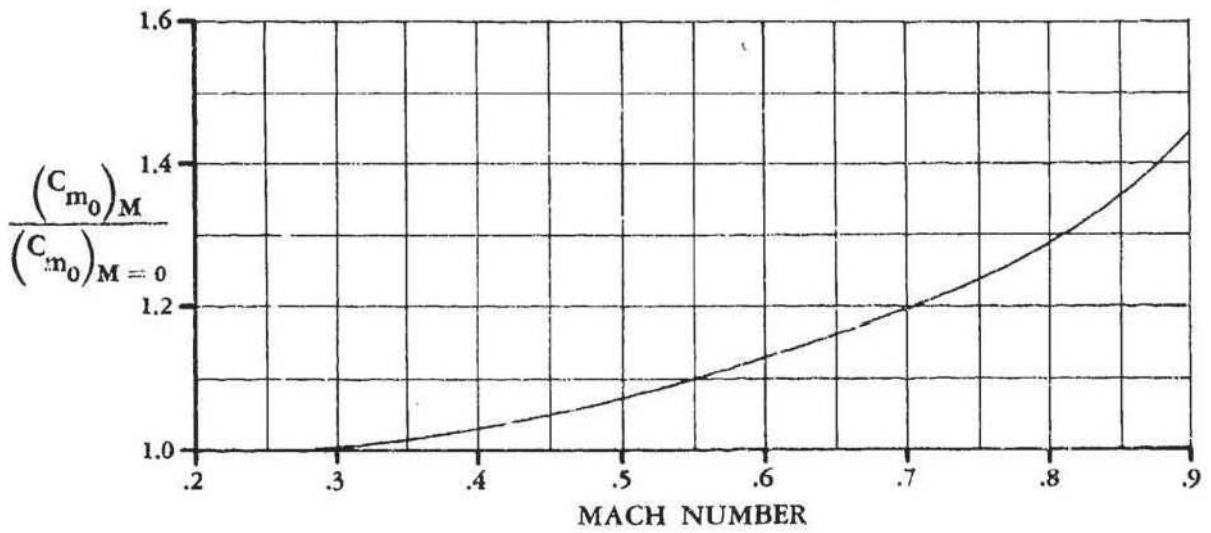


Figure 25 - Effect of Compressibility on the Wing Zero-Lift Pitching-Moment Coefficient

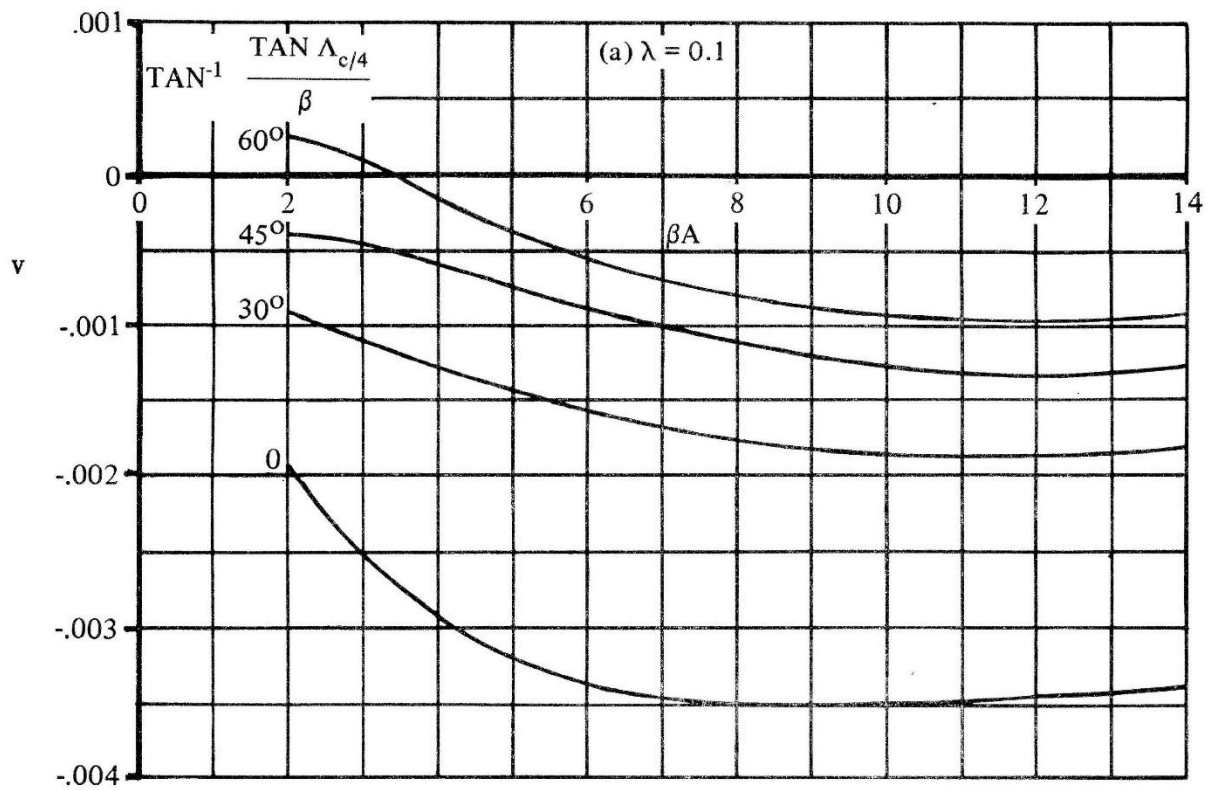


Figure 26. Lift dependent drag factor due to linear twist, ($\lambda=0.1$)

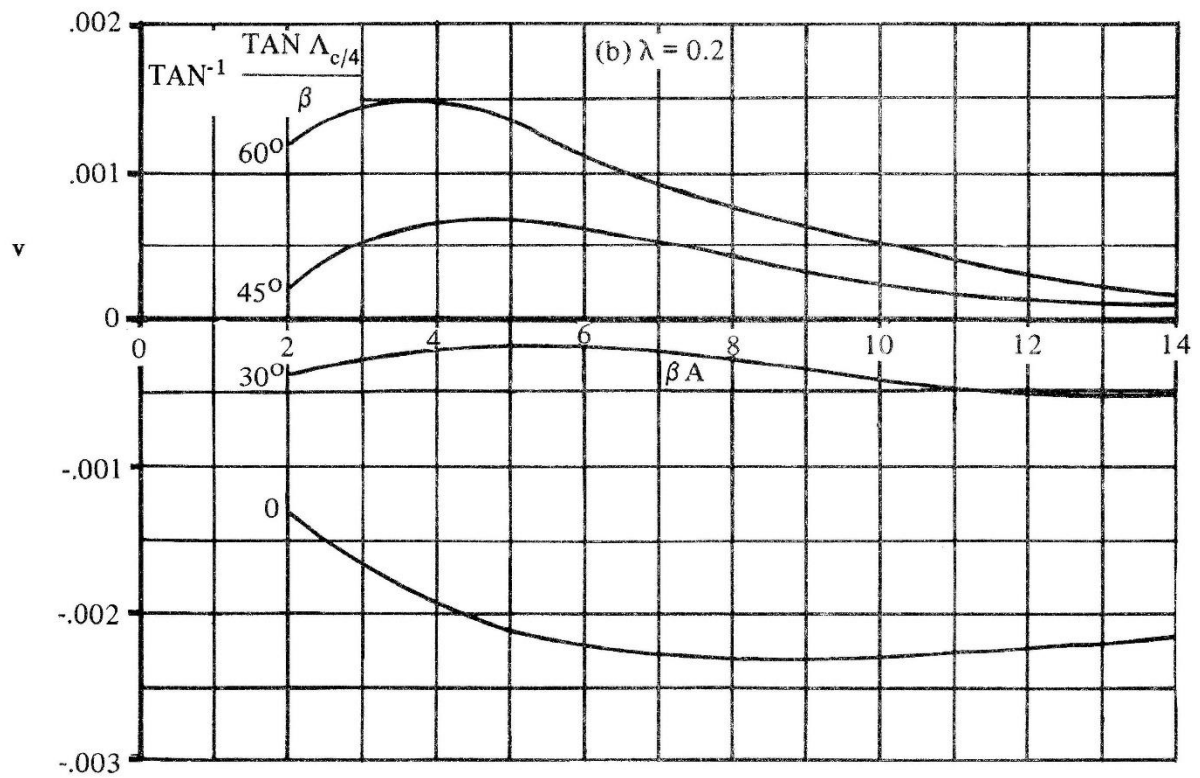


Figure 27. Lift dependent drag factor due to linear twist, ($\lambda=0.2$)

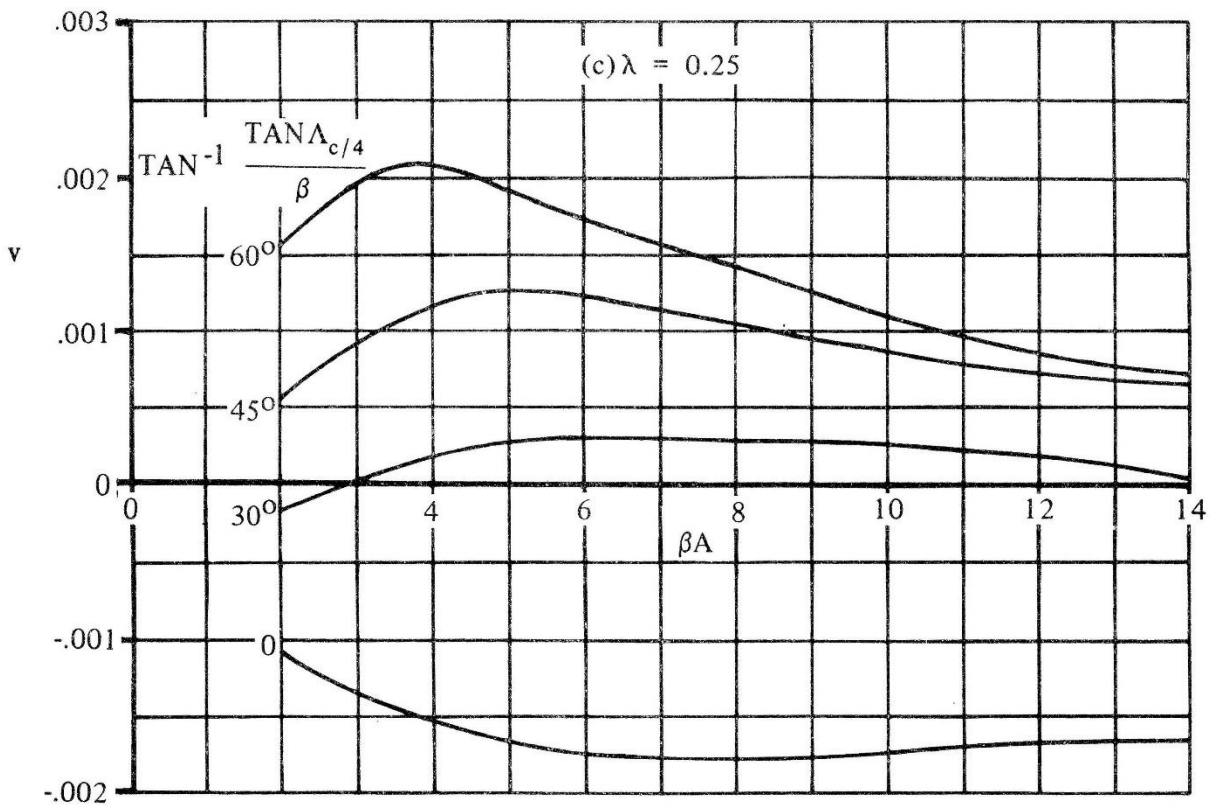


Figure 28. Lift dependent drag factor due to linear twist, ($\lambda=0.25$)

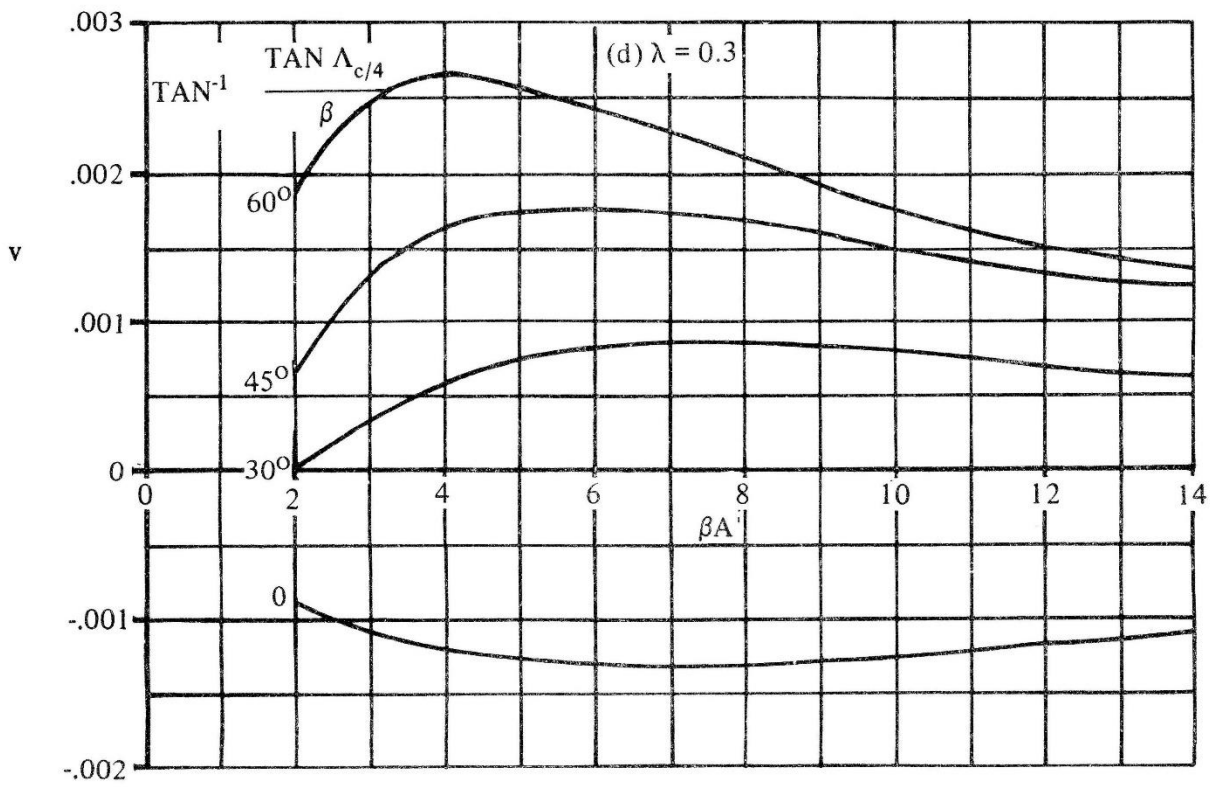


Figure 29. Lift dependent drag factor due to linear twist, ($\lambda=0.3$)

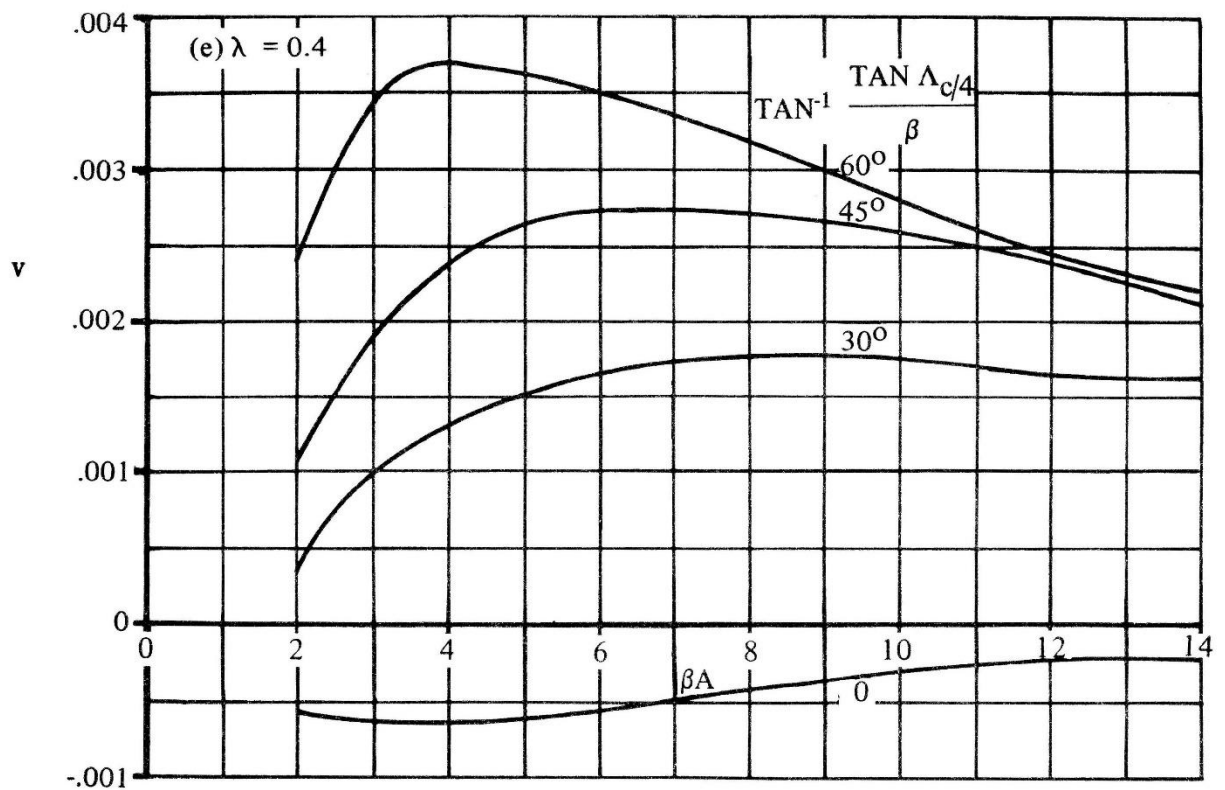


Figure 30. Lift dependent drag factor due to linear twist, ($\lambda=0.4$)

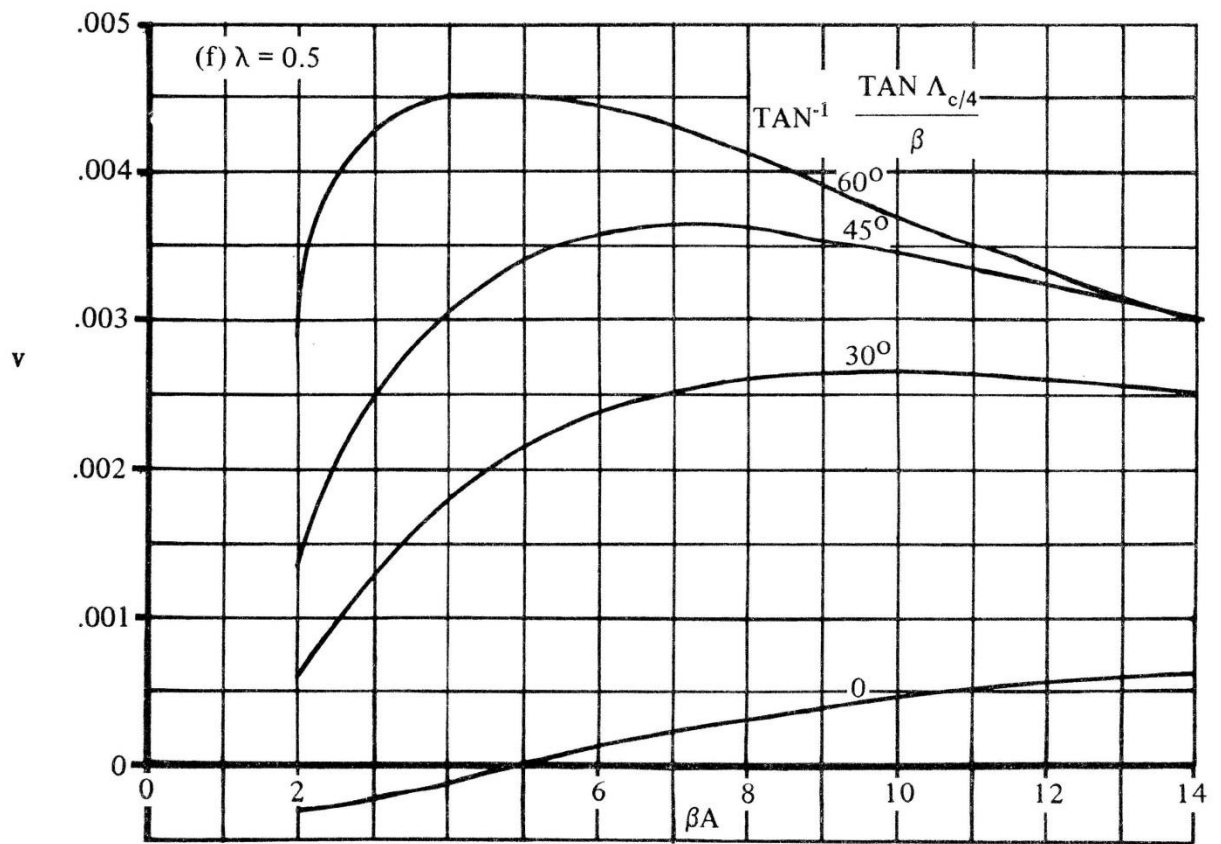


Figure 31. Lift dependent drag factor due to linear twist, ($\lambda=0.5$)

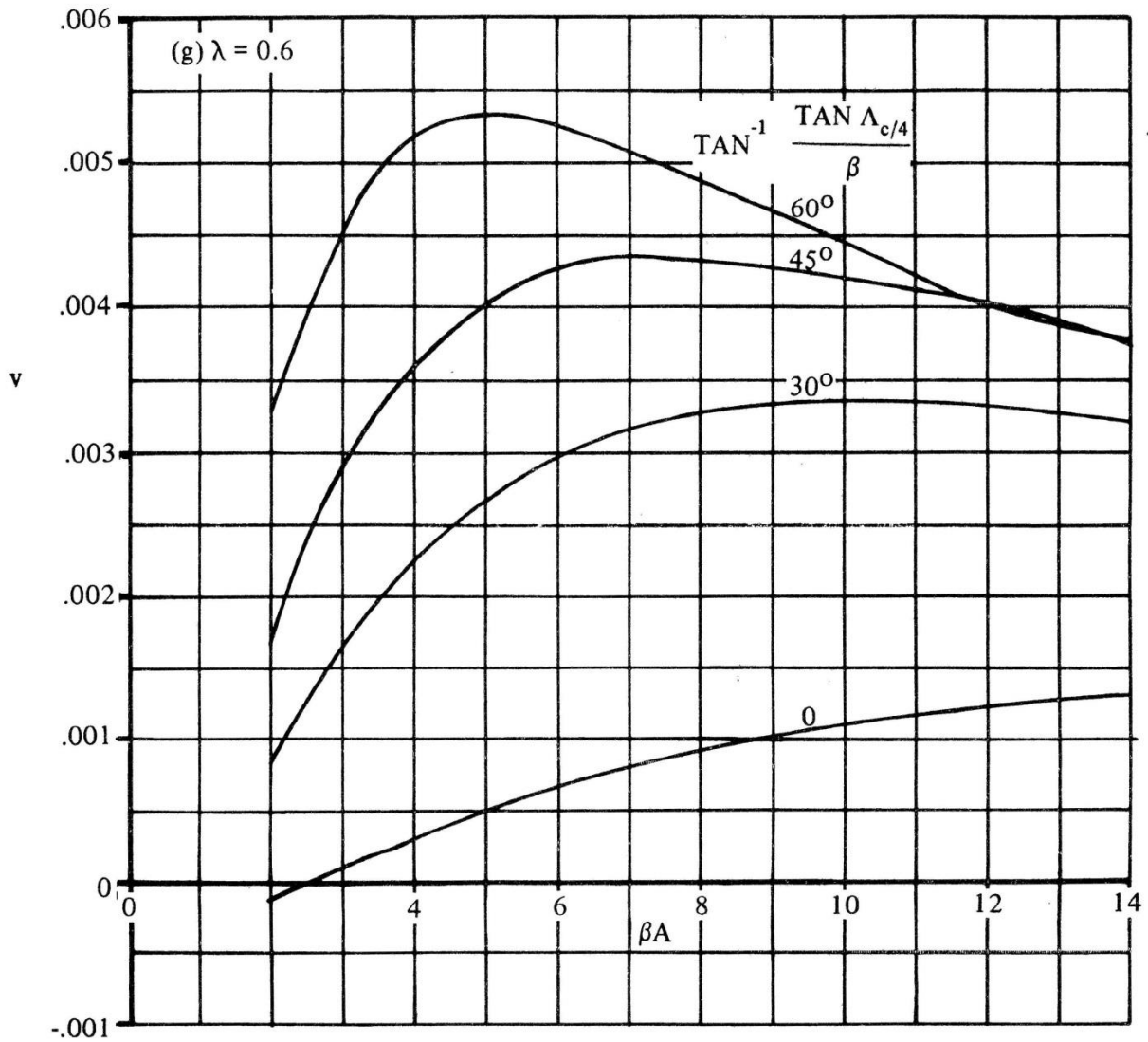


Figure 32. Lift dependent drag factor due to linear twist, ($\lambda=0.6$)

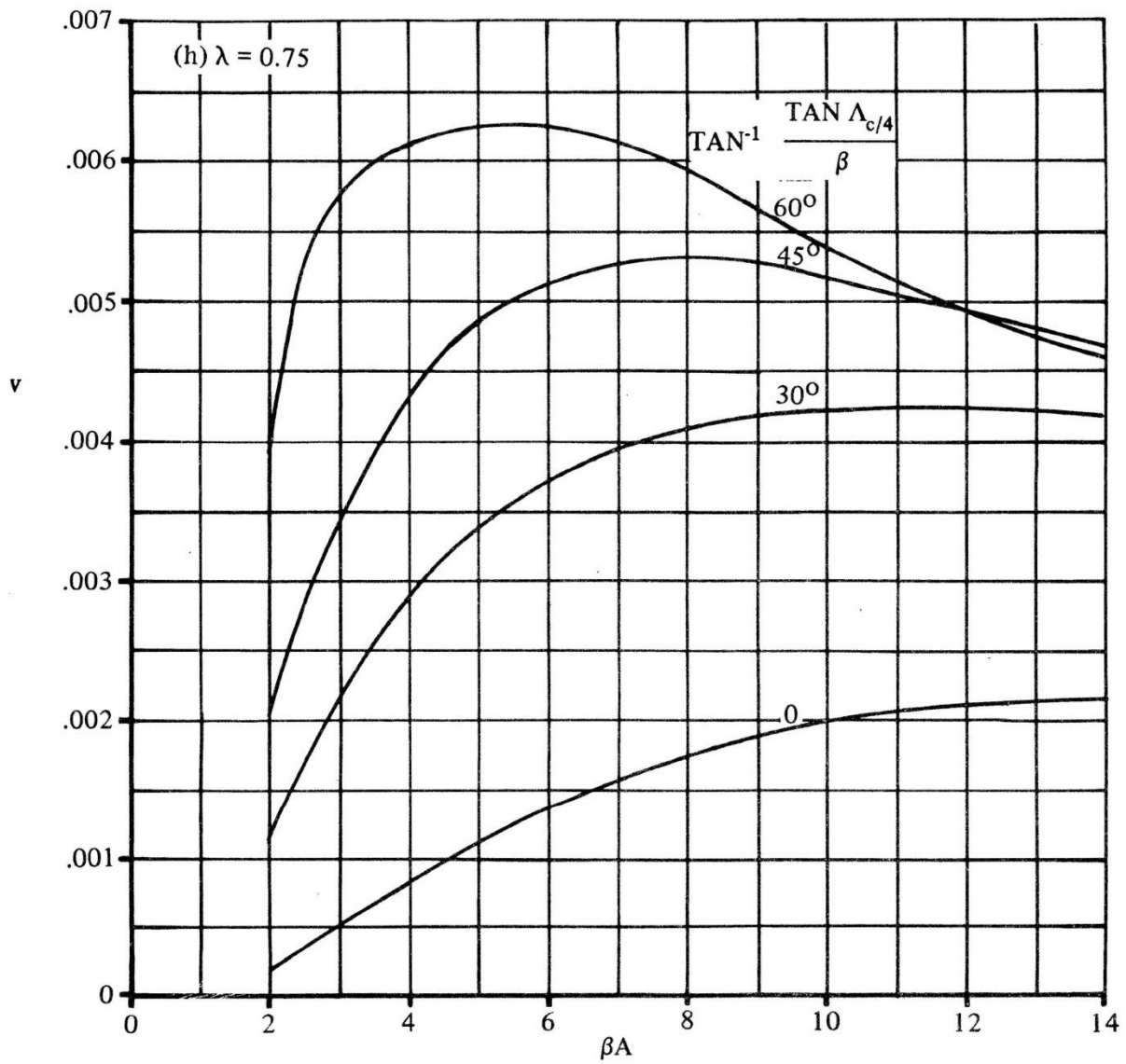


Figure 33. Lift dependent drag factor due to linear twist, ($\lambda=0.75$)

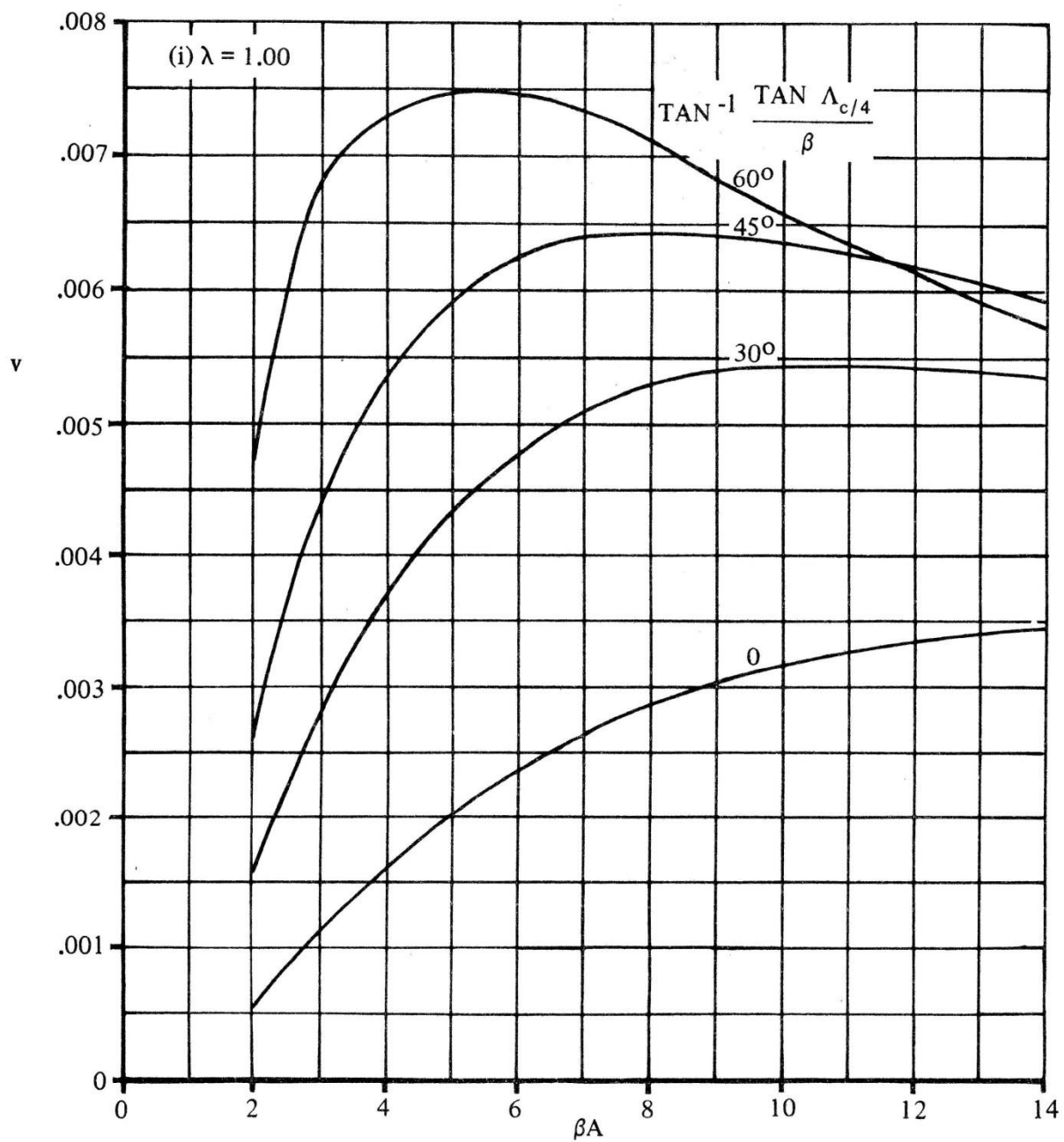


Figure 34. Lift dependent drag factor due to linear twist, ($\lambda=1.0$)

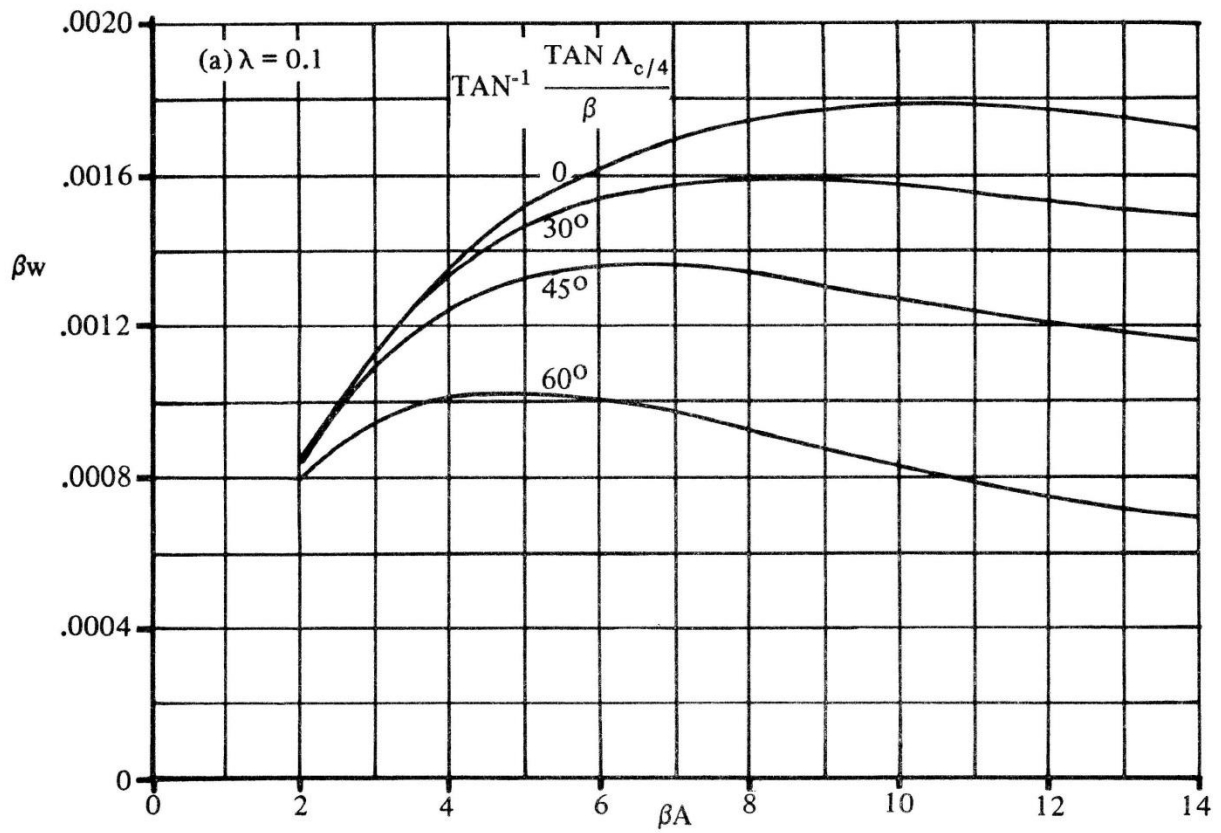


Figure 35. Zero lift drag factor due to linear twist, ($\lambda=0.1$)

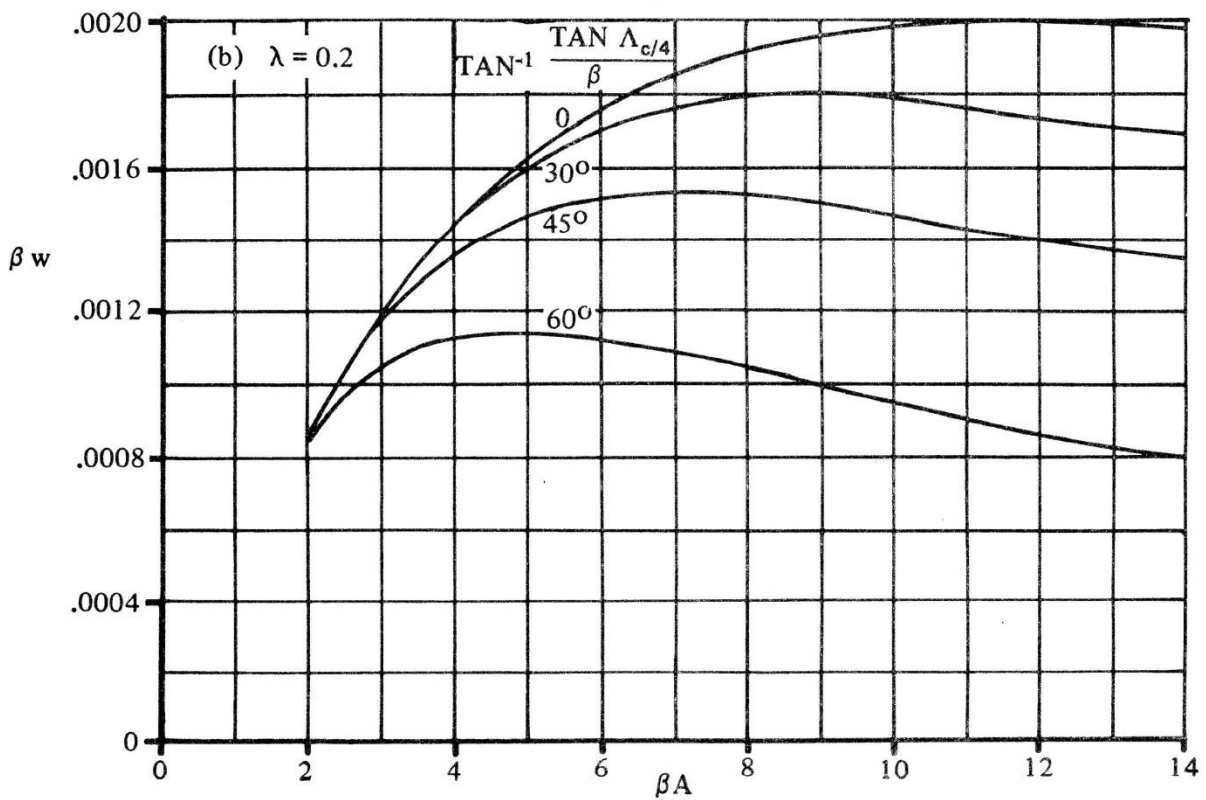


Figure 36. Zero lift drag factor due to linear twist, ($\lambda=0.2$)

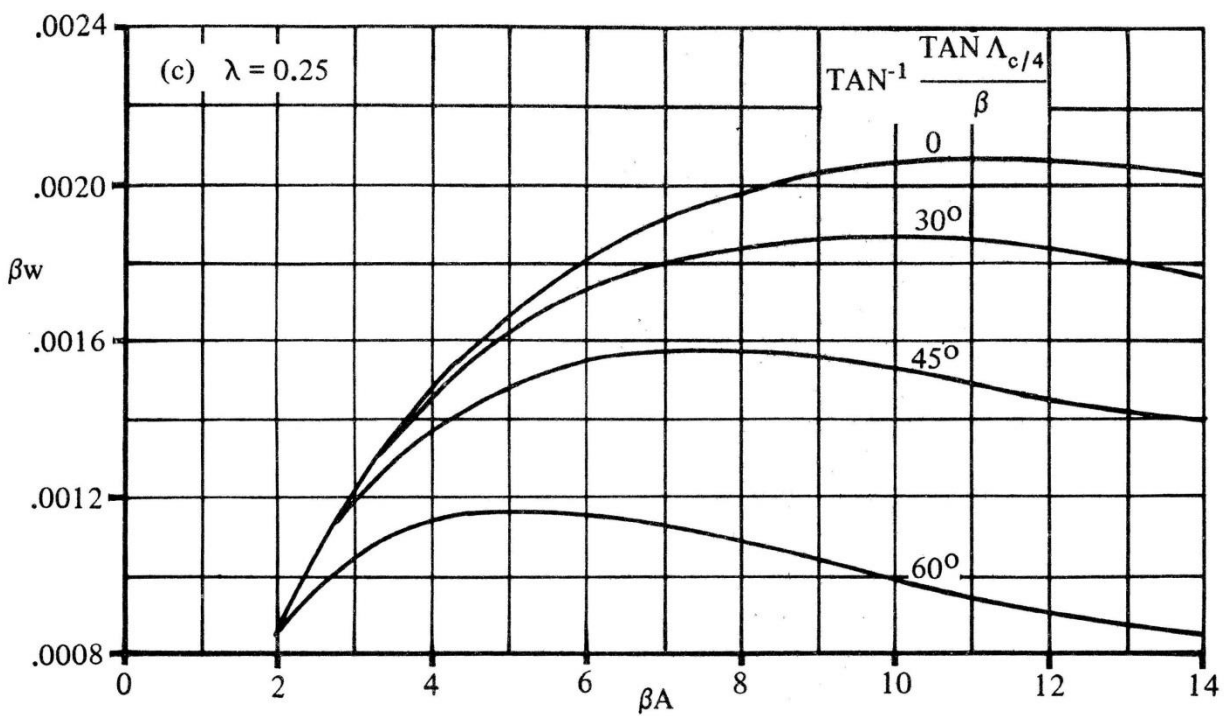


Figure 37. Zero lift drag factor due to linear twist, ($\lambda=0.25$)

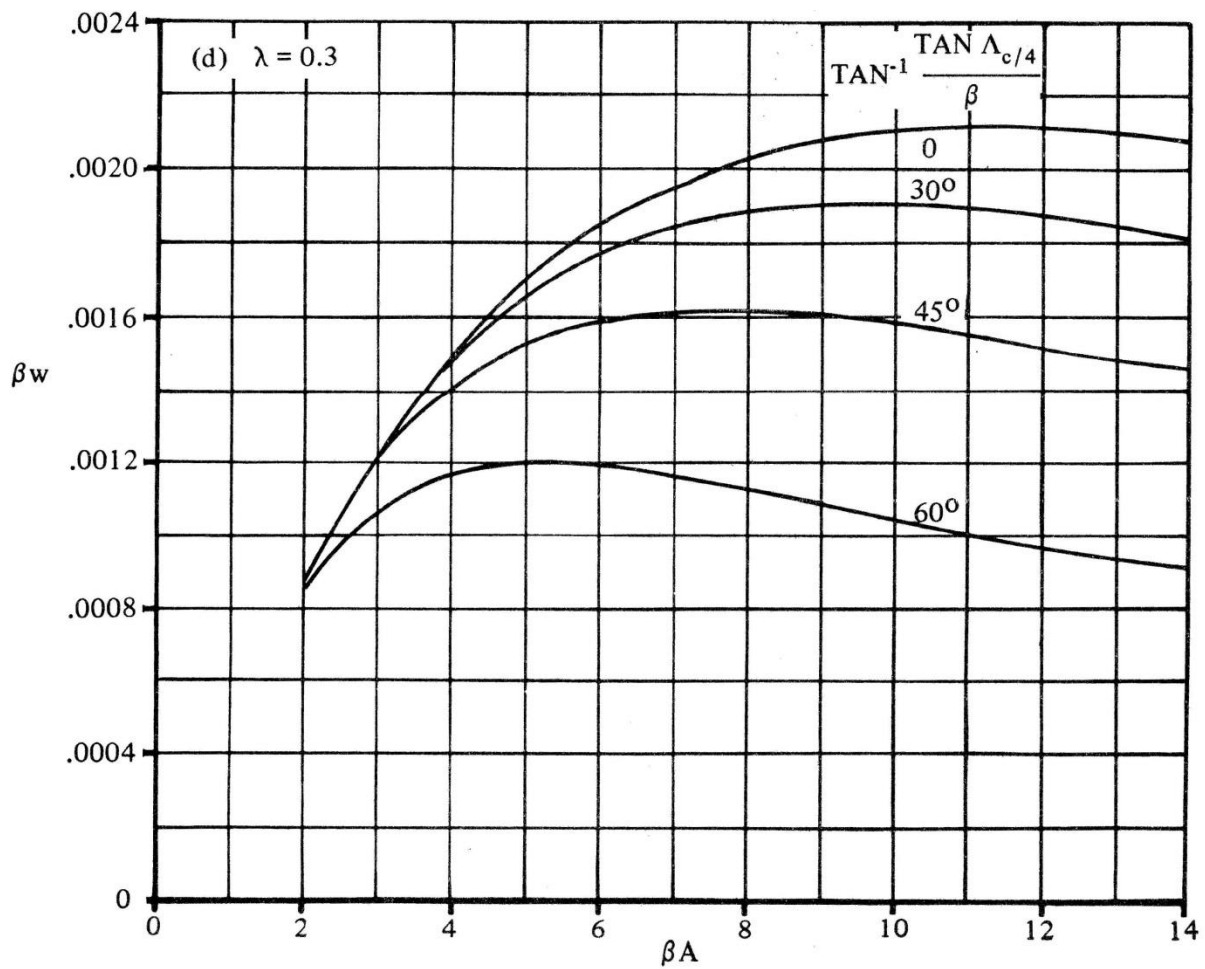


Figure 38. Zero lift drag factor due to linear twist, ($\lambda=0.3$)

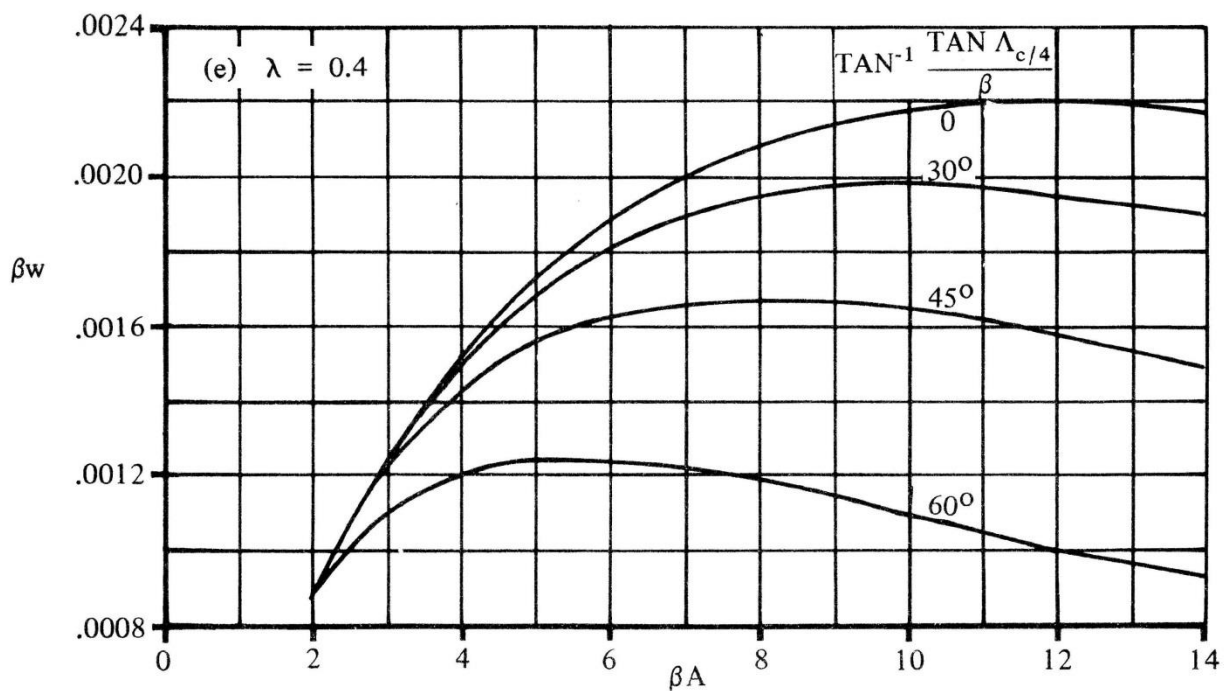


Figure 39. Zero lift drag factor due to linear twist, ($\lambda=0.4$)

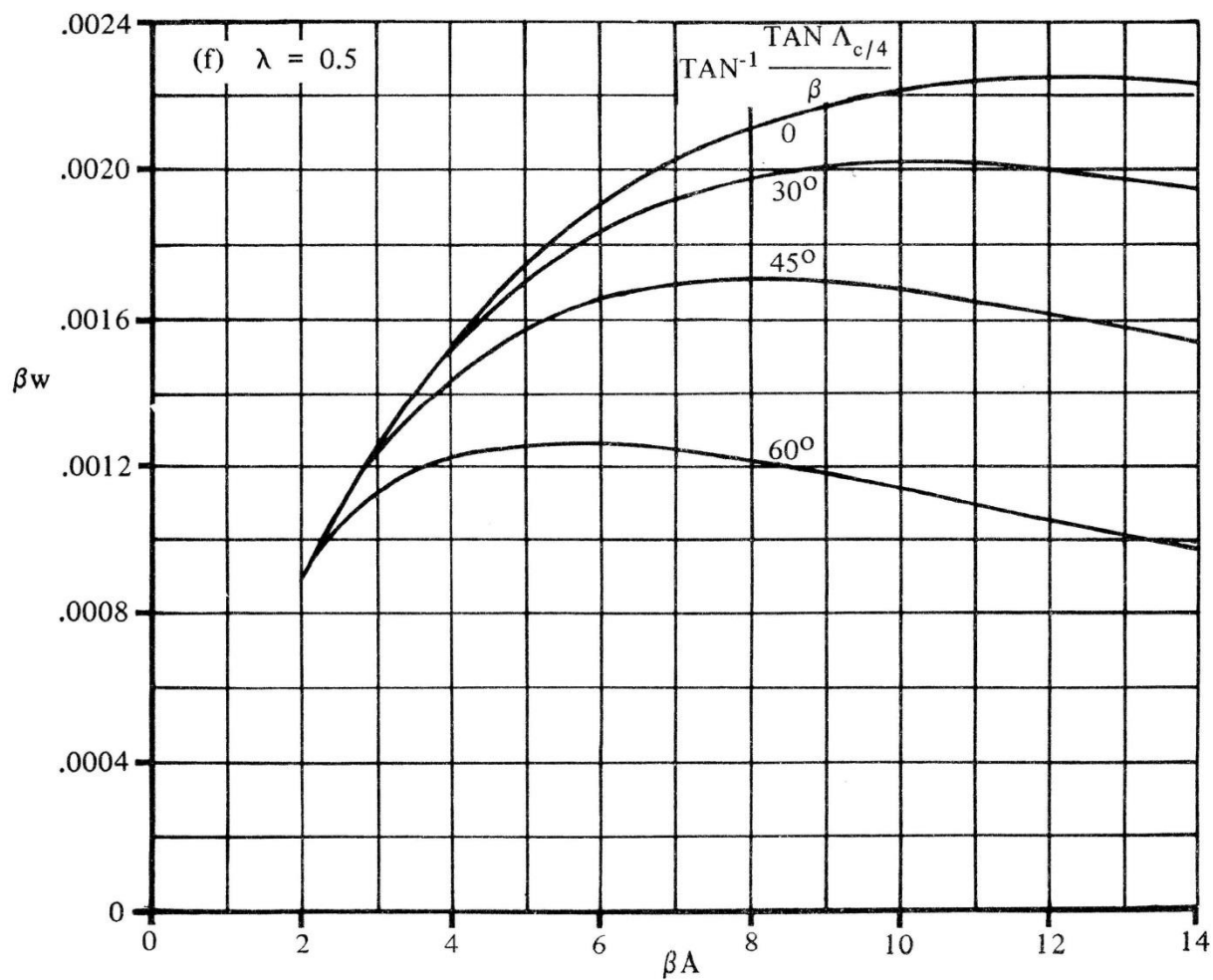


Figure 40. Zero lift drag factor due to linear twist, ($\lambda=0.5$)

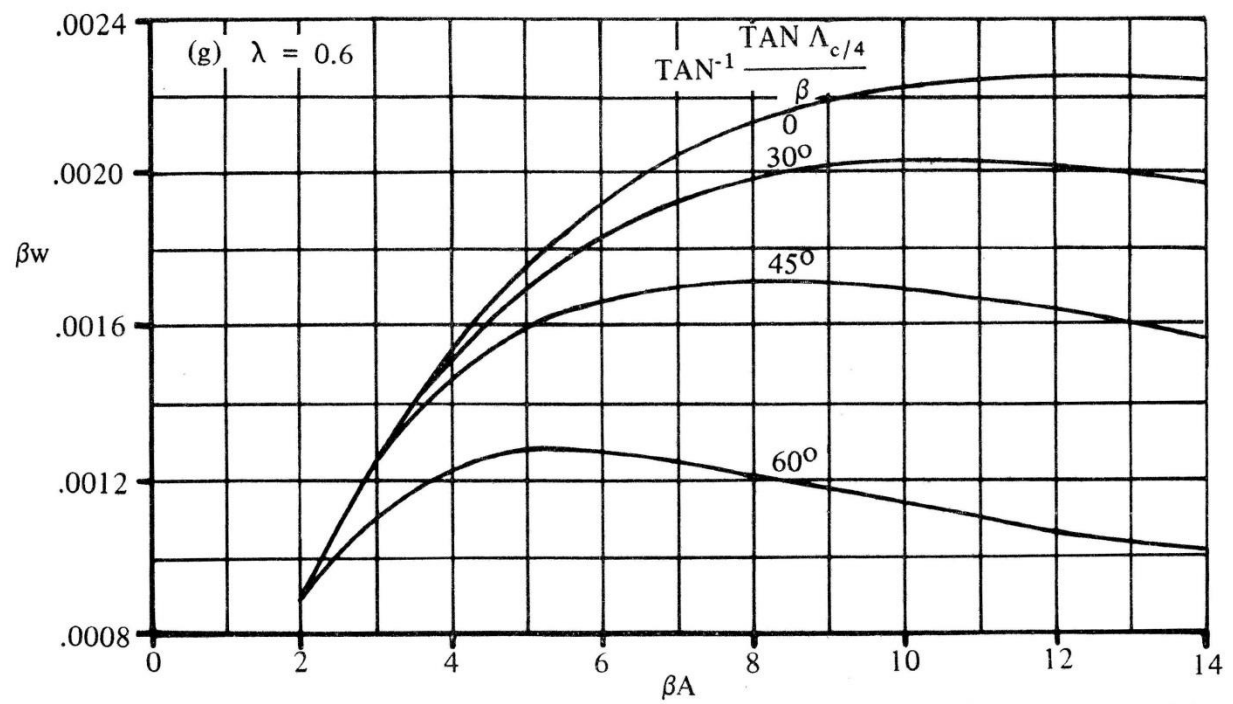


Figure 41. Zero lift drag factor due to linear twist, ($\lambda=0.6$)

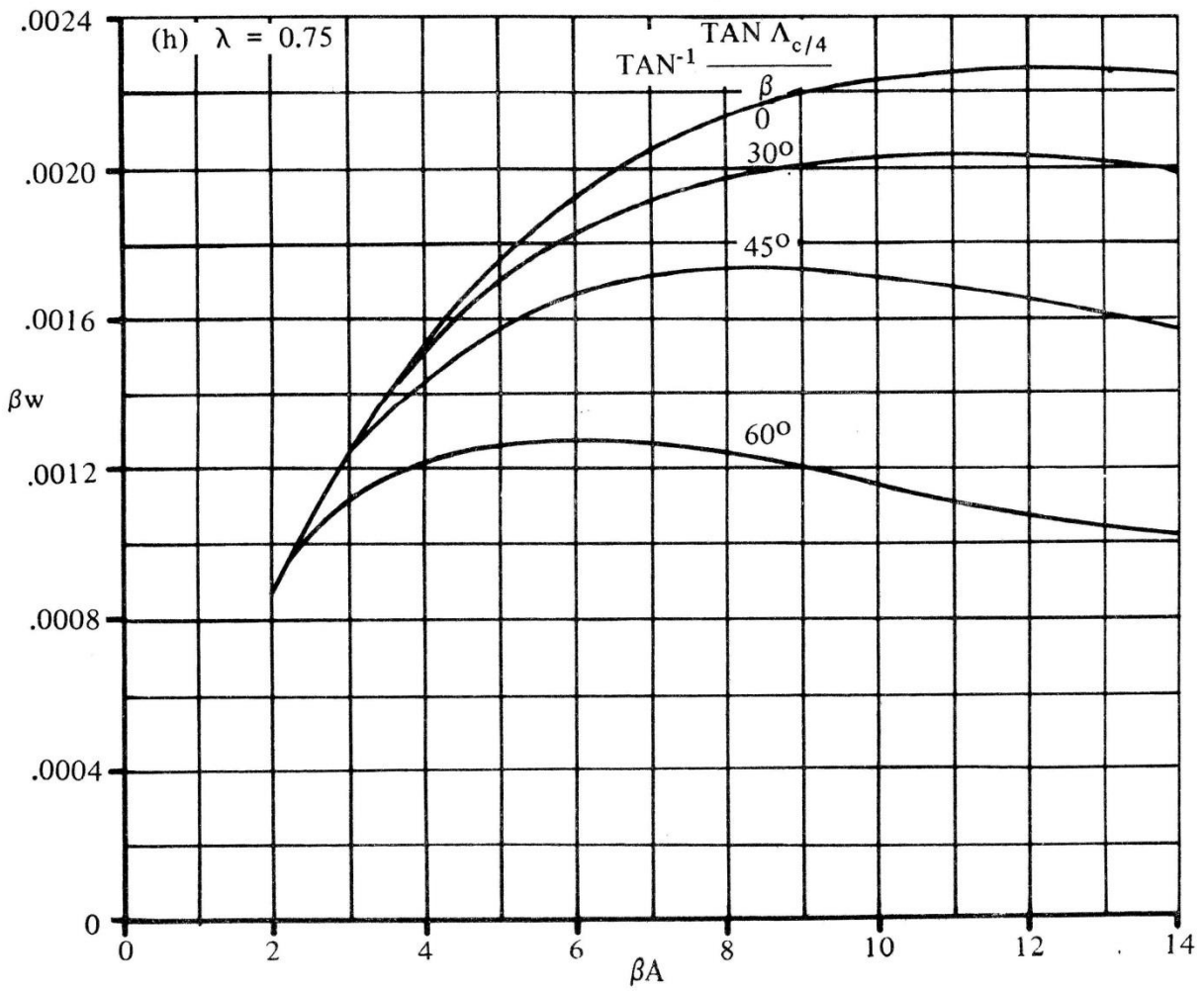


Figure 42. Zero lift drag factor due to linear twist, ($\lambda=0.75$)

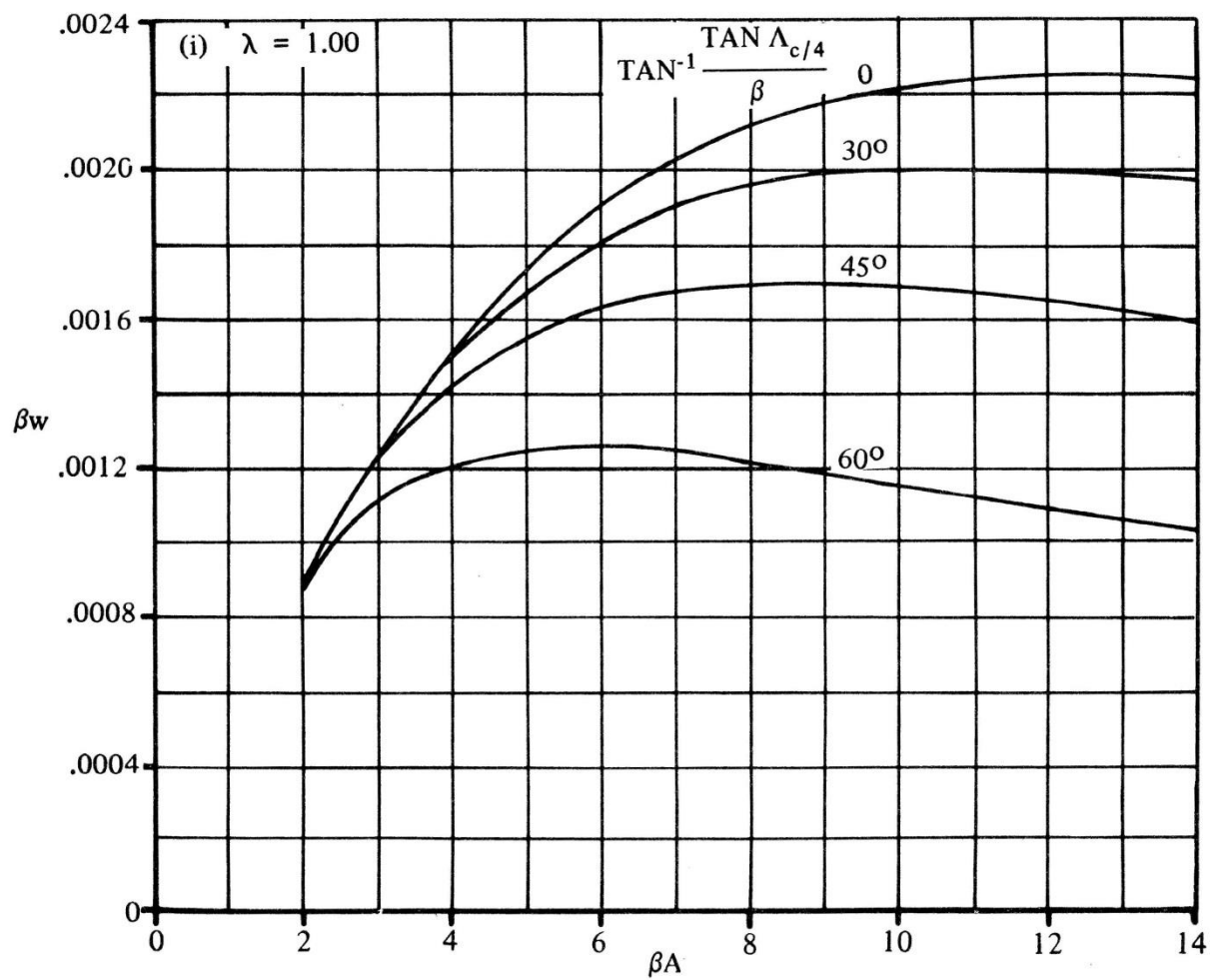


Figure 43. Zero lift drag factor due to linear twist, ($\lambda=1.0$)

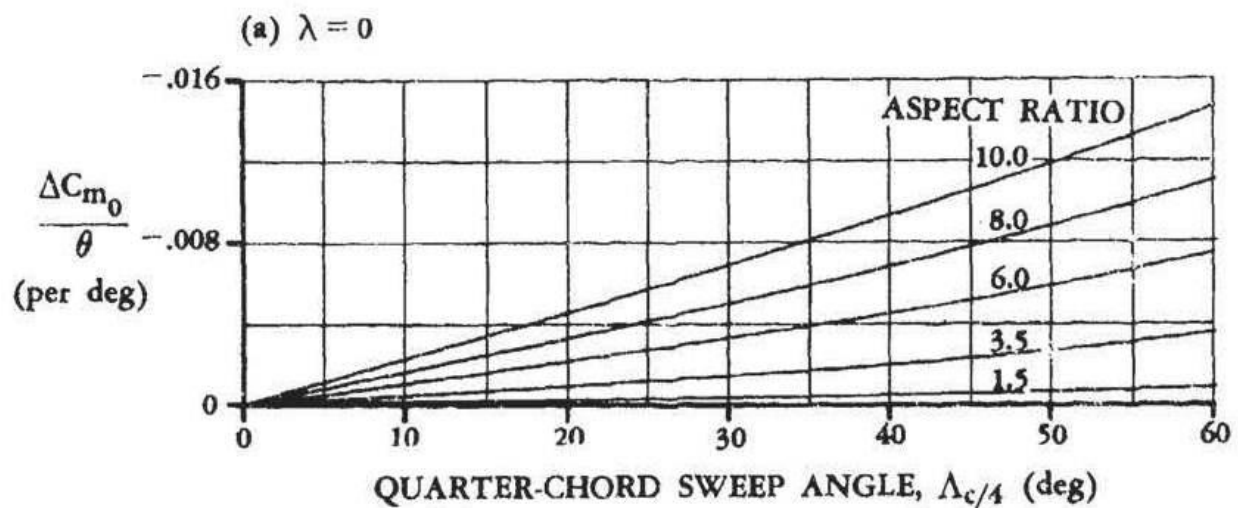


Figure 44 - Effect of Linear Twist on the Zero-Lift Pitching Moment, ($\lambda=0$)

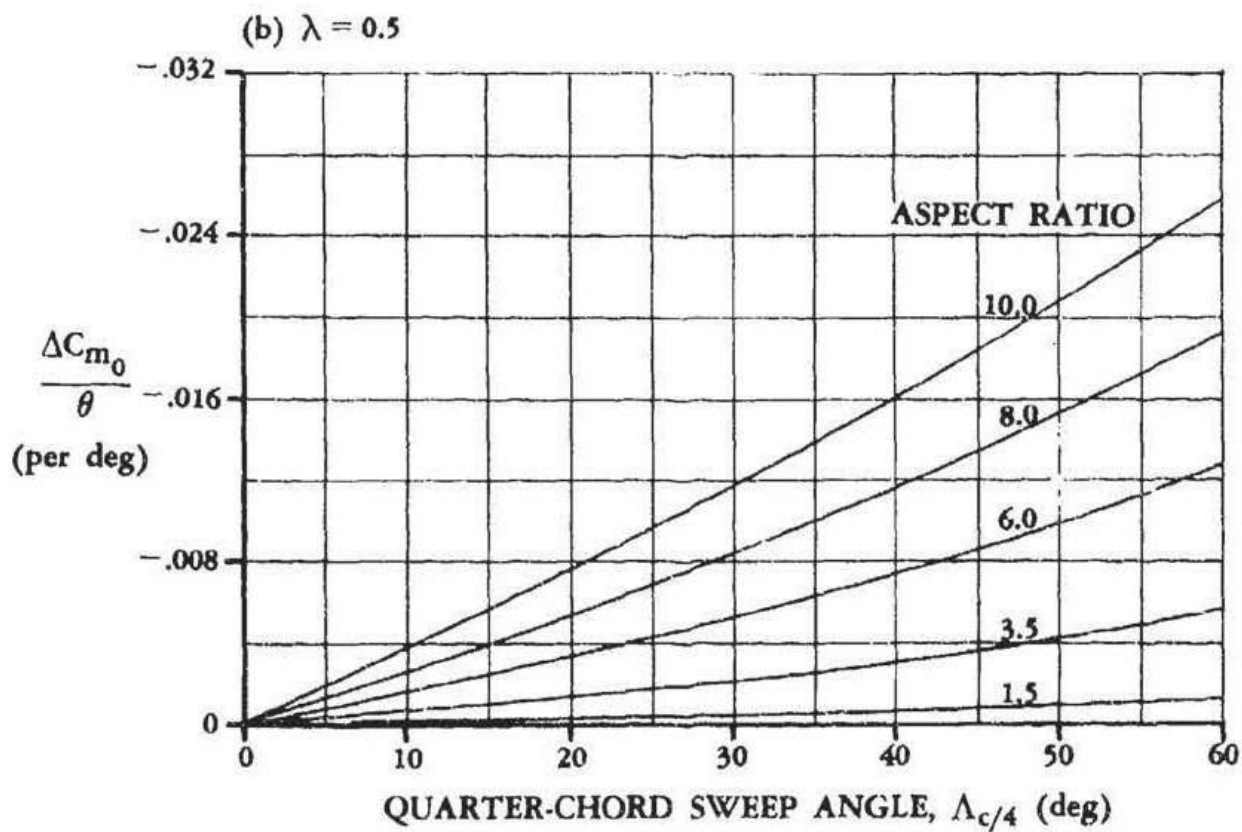


Figure 45 - Effect of Linear Twist on the Zero-Lift Pitching Moment, ($\lambda=0.5$)

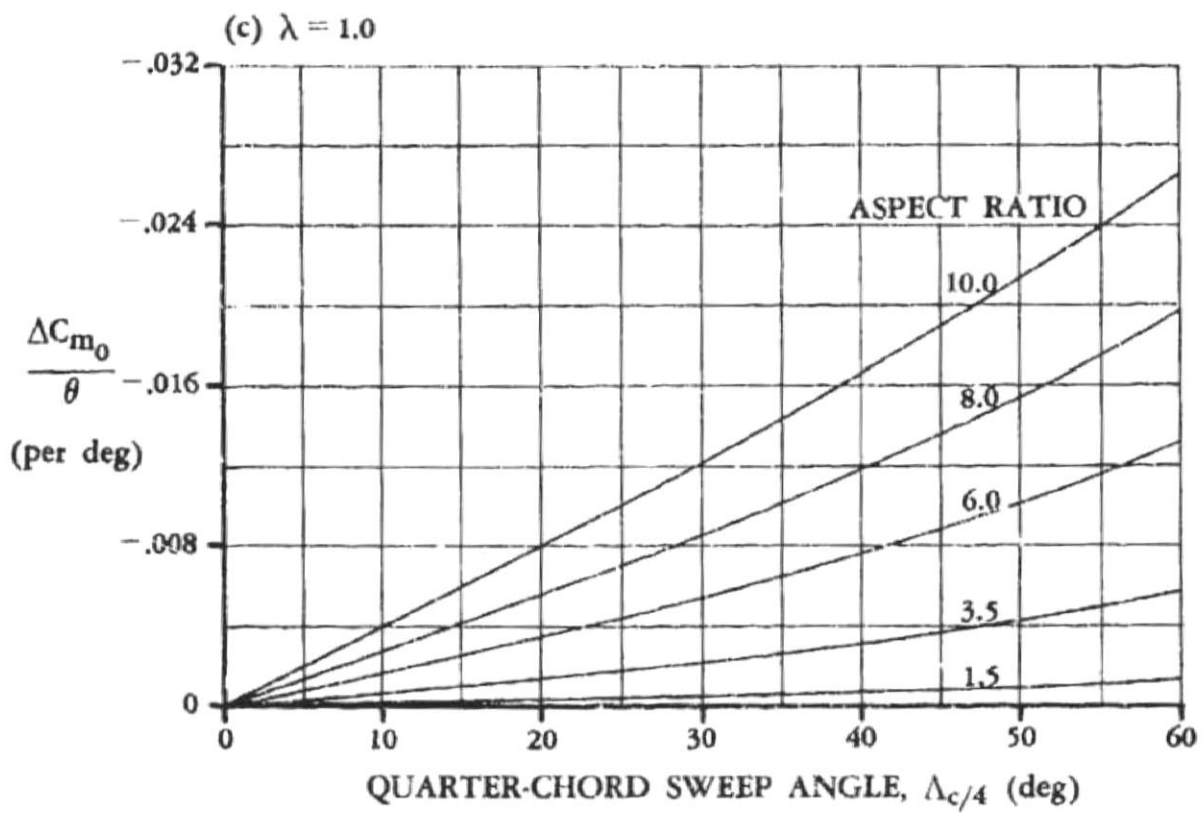


Figure 46 - Effect of Linear Twist on the Zero-Lift Pitching Moment, ($\lambda=1.0$)